

Exploring the possibilities of using Active Rear Steering in a car

*Master of Science Thesis in the Master Degree Programme, Systems,
Control & Mechatronics*

JONAS ARVIDSSON
ERIC FRANKLIN

Department of Signals & Systems
CHALMERS UNIVERSITY OF TECHNOLOGY
Göteborg, Sweden, 2012
Report No. EX039/2012

Exploring the possibilities of using Active Rear Steering in a car

Master Thesis in Systems, Control & Mechatronics

Jonas Arvidsson
Eric Franklin

Department of Signals and Systems
CHALMERS UNIVERSITY OF TECHNOLOGY
Göteborg, Sweden, 2012

Exploring the possibilities of using Active Rear Steering in a car

Master Thesis in Systems, Control & Mechatronics

JONAS ARVIDSSON

ERIC FRANKLIN

© JONAS ARVIDSSON, ERIC FRANKLIN 2012

Technical report no: EX039/2012

Department of Signals & Systems

Chalmers University of Technology

SE-412 96 Göteborg

Sweden

Telephone + 46 (0)31-772 1000

Cover:

Isometric view of Two Track model, see section 3.2.

Abstract

In this master thesis the possibilities of using *Active Rear Steering* (ARS) in a car is investigated. The aims of the thesis are to improve maneuverability in low speeds and make the car more stable in high speeds. A Two Track model is derived and implemented in MATLAB/Simulink and is used as a simulation model of a real vehicle. Two types of controllers are used, a proportional gain (K_p) is used to improve maneuverability in low speeds and an LQ-controller for stability in high speeds. The high-speed controller utilizes a reference which is a first order transfer function which approximates the yaw rate depending on the steering wheel angle and the vehicle's velocity.

An existing parallel parking algorithm is modified to incorporate rear wheel steering to investigate if ARS contributes enough to be implemented in automatic parking. The parallel parking algorithm uses sinusoidal functions to calculate control signals for steering and velocity. The algorithm searches iteratively for a suitable collision-free path that moves the car as close as possible to a desired end position.

The maneuverability is improved in low speeds and the effect got more apparent when the maximum rear steer angle is increased. However, ARS has negative impact in the current parallel parking algorithm. With a more advanced algorithm it may be possible to utilize ARS more efficiently. The behavior of the car in high speeds is highly dependent of the reference model. It is possible to adjust the reference model in order to make the car more stable or more agile.

Preface

The master thesis is a part of the VESC-programme (“Volvos Examens- & Sommarjobb för Chalmerister”). It is a collaboration between Volvo Car Corporation (VCC) and Chalmers students looking for a summer job and a master thesis. The summer of 2011 we worked at VCC and started developing a mathematical model of a four wheel steered car.

Acknowledgment

First of all we would like to thank Volvo Cars for the opportunity to participate in the VESC-programme. Furthermore we would like to thank our supervisors Andreas Eriksson and Peter Wennberg at Volvo Cars and Jonas Fredriksson at Chalmers. We would like to thank Jan Hellberg at Volvo Cars and Mathias Lidberg at Chalmers for the support on modeling and validation. A special thanks to Torsten Wik at Chalmers for help and discussions about control design.

Contents

1	Introduction	1
1.1	Background	1
1.2	Purpose and goals	1
1.3	Delimitations	2
2	Methods	3
2.1	Evaluation of low- and high-speed driving cases	3
2.2	Parallel parking	4
3	Mathematical models	5
3.1	Bicycle model	5
3.1.1	Lagrange equations	6
3.1.2	Nonlinear Bicycle Model and the Magic Formula	8
3.2	Two Track model	10
3.2.1	Lagrange equations	11
3.2.2	Kinetic energy	13
3.2.3	Potential energy	15
3.2.4	Self-aligning torque	15
3.2.5	Load transfer	16
3.2.6	Final state equations	17
4	Control design	18
4.1	Low speed	18
4.2	High speed stability	18
4.3	Parallel parking algorithm	19
4.3.1	Algorithm	20
5	Simulations	23
5.1	Model validation	23
5.1.1	Sine 0.5 Hz	23
5.1.2	Sine with dwell	26
5.2	Low speed simulations	27
5.2.1	Minimum turn radius	28
5.2.2	S-curve	28
5.2.3	Follow S-curve	29
5.2.4	Take-off from parallel parking	31
5.3	High speed simulations	33
5.3.1	Step steer	33
5.3.2	Lane change	36
5.3.3	External lateral force	39
5.4	Parallel parking algorithm	40
6	Conclusion	45
6.1	Future work	46
	References	47
A	Linear Bicycle model	I

B Two Track model: Equations	I
B.1 Total kinetic energy	I
B.2 Derivatives of Lagrange equations of motion	II
B.3 Final state equations	III
C Driving cases	IV
C.1 Minimum turn radius	IV
C.2 S-curve	IV
C.3 Follow S-curve	IV
C.4 Take-off from parallel parking	V
C.5 Step steer	V
C.6 Lane change	V
C.7 External lateral force	VI
C.8 Sine 0.5 Hz	VI
C.9 Sine with dwell	VI
D Low speed simulations	VIII
D.1 Take-off from parallel parking	VIII
E High speed simulations	IX
E.1 Step steer	IX

Variables

The variables used in the master thesis are presented in this section. They are divided into “Common”, “Bicycle model”, “Two Track model” and “Parallel parking algorithm”.

Common

s_f, s_r	wheel angle of front and rear wheel
a, b	distance from center of gravity to front and rear axle
m	the car's total mass
CM	center of mass
u	longitudinal velocity relative car
v	lateral velocity relative car
V	resulting velocity relative car
ψ	yaw angle
φ	roll angle
x, y	absolute position of the car in the global coordinate system
B_f, B_r	stiffness factor front and rear (Magic formula)
C_f, C_r	shape factor (Magic formula)
D_f, D_r	peak value front and rear (Magic formula)
E_f, E_r	curvature factor front and rear (Magic formula)
$C_{stiff_f,r}$	cornering stiffness front and rear

Bicycle model

F_{yf}, F_{yr}	lateral tire forces on front and rear wheel
δ_f, δ_r	slip angle of front and rear wheel

Two Track model

A	point beneath CM when roll angle is 0
B	point where the body rolls about
s_i	wheel angle of wheel i
tw_f, tw_r	track width front and rear
θ	roll axis inclination angle
δ_i	slip angle of wheel i
$F_{x,i}$	longitudinal tire force on wheel i
$F_{y,i}$	lateral tire force on wheel i
$F_{z,i}$	vertical force on wheel i
$M_{z,i}$	self-aligning torque on wheel i
$Pneu_i$	pneumatic trail of wheel i
$Mech_i$	mechanical trail of wheel i
$Caster_i$	caster angle of wheel i
T	kinetic energy
U	total potential energy
U_s	spring energy
U_g	gravity energy
Q_i	non-conservative force in direction i
rc_f, rc_r	roll center front and rear
h'	distance between CM and B
h_r, h_f	height of roll center front and rear
$c_{\varphi f}, c_{\varphi r}$	roll stiffness front and rear
$k_{\varphi f}, k_{\varphi r}$	roll damping coefficient front and rear
e^i	reference frame $i = 0..4$
ω	rotational speed of reference frame 3 compared to frame 0 expressed in reference frame 4

Parallel parking algorithm

β	side-slip angle
t'	total time for maximum steering
T^*	sinusoidal transition period
T	total time for one iterative parking maneuver
$D_{l,w}$	available parking space illustrated in figure 7
x_{margin}	margin to the parked cars front and rear
y_{margin}	margin to the wall or curb
$overhang_{rear}$	length from rear axle to rear end of car

1 Introduction

The master thesis is presented in this section. The background, goals, objectives and delimitations will be described in detail.

1.1 Background

Safety in cars is both a selling point and a necessity for today's leading car manufacturers. The focus has been drawn from only passive safety to both passive and active safety. Passive safety is trying to prevent passenger injury when an accident occurs, while active safety tries to avoid accidents and collisions before they happen. Another trend is that new cars are equipped with wider and larger tire and rims that could lead to larger turn radius.

To deal with the tasks and problems mentioned above a few car manufacturers have implemented *Active Rear Steering* (ARS) such as BMW, Lexus and Renault. One of the first manufactured cars with ARS was the Nissan Skyline introduced in the mid 1980:s. The early car models rear wheels' motion were a function of the steering wheel angle via a mechanical link. With the help of electric actuators and sensors ARS could theoretically give both better maneuverability in low speeds and stability in high speeds. Volvo Car Corporation (VCC) is reviewing the possibilities of implementing ARS in some of their future car models.

This master thesis aims to explore the possibilities of using ARS in a car both in low and high speeds.

1.2 Purpose and goals

The purpose of the master thesis is to present the effects and possibilities of using ARS in different driving situations such as parallel-parking, low- and high-speed maneuvers. It will also give recommendations for the next steps when implementing ARS in a car and potential problems that could occur.

To achieve the proposed end effects the goals are to:

- Derive a nonlinear mathematical model that represents a car with four wheel steering.
- Analyze common low speed ($<10 \text{ km/h}$) driving situations and evaluate the possible benefits of ARS, as well as look into a special case (take-off from parallel parking) described in section C.4.
- Analyze high-speed maneuvers ($70 - 130 \text{ km/h}$) and make the car more stable with the help of ARS.
- Design a control principle that could be used as a base for implementation in a real vehicle.
- Derive a path-planning algorithm for parallel parking that utilizes the ARS. The algorithm should minimize the number of cusps. Evaluate if ARS contributes enough to be implemented in automatic parallel parking.

1.3 Delimitations

The following delimitations has been set up:

- The research is limited to a number of specified driving cases both in low and high speeds.
- The derived control principles are meant as guidelines and not to be directly implemented in a vehicle.
- The surface is assumed to be flat in the simulations.

2 Methods

In this section the methods used in the master thesis are presented and explained. A number of test cases will be presented to evaluate the possibility for better maneuverability and stability using ARS. However, it is hard to determine good vehicle dynamics through simulations because it is highly subjective, thereby physical tests are recommended.

2.1 Evaluation of low- and high-speed driving cases

The Two Track model, derived in 3.2, will be used as a simulation model in MATLAB and Simulink. The derived model will first be validated with the help of a VI-CarRealTime-model (see section 5.1).

Different low- and high-speed driving cases will be simulated. In table 1 the different cases are presented with a description of the case's contribution. For more detailed information of the cases see Appendix C.

Driving case	Contribution	Info
Low speed		
Minimum turn radius	Difference in turn radius	C.1
S-curve side transfer	Difference in maneuverability	C.2
Follow S-curve	Steer angle difference	C.3
Take-off from parallel parking	Lateral displacement	C.4
High speed		
Step steer	Responsiveness and stability	C.5
Lane change	Stability and lateral displacement	C.6
External lateral force	Stability and lateral displacement	C.7

Table 1: Driving cases and description.

The low speed driving situations are focused on maneuverability and a special case where the car is parked close along a wall or curb. The latter will show if there is any risk of colliding with the obstacle because of the implementation of ARS.

Stability is the main focus for the high-speed maneuvers. A control law will be implemented in the simulation environment to stabilize the car to follow a reference model. A simpler model than the Two Track will be used as reference model.

2.2 Parallel parking

A path-planning algorithm is going to be used to evaluate if the contribution of ARS is large enough for implementing rear wheel steering in an already existing parking system. The algorithm is based on the one suggested by Laugier and Paromtchik [2], described in section 4.3. The algorithm is going to be modified to use ARS during the parking maneuver. This will be implemented and simulated in MATLAB and Simulink.

3 Mathematical models

In almost every case when designing a mechatronic system, simulation of the system is performed. To simulate a car a mathematical model is needed to describe its motion. There are several types of models that can be used, the simplest is the Bicycle model that is conformed around that the car only has one front and one rear wheel i.e. as a bicycle. In its simplest form the Bicycle model has only two degrees of freedom, lateral velocity and yaw rate. It can be extended with more degrees of freedom such as roll. The Bicycle model may not be accurate enough, then the Two Track or a more advanced model can be used instead. The Two Track utilizes all four wheels and has four main degrees of freedom: longitudinal and lateral velocity, roll and yaw rate.

Both the Bicycle and Two Track model are derived. The Bicycle model is used when designing the LQ-controller (see section 4.2). The Two Track model is implemented in Simulink to be used as a representation of a real car (see section 3.2).

3.1 Bicycle model

The Bicycle model is a relatively simple model that describes a basic car's motions. The advantages with this model is that it has few degrees of freedom and it is easy to grasp. The drawback is that it is not as precise as the more advanced models in extreme maneuvers.

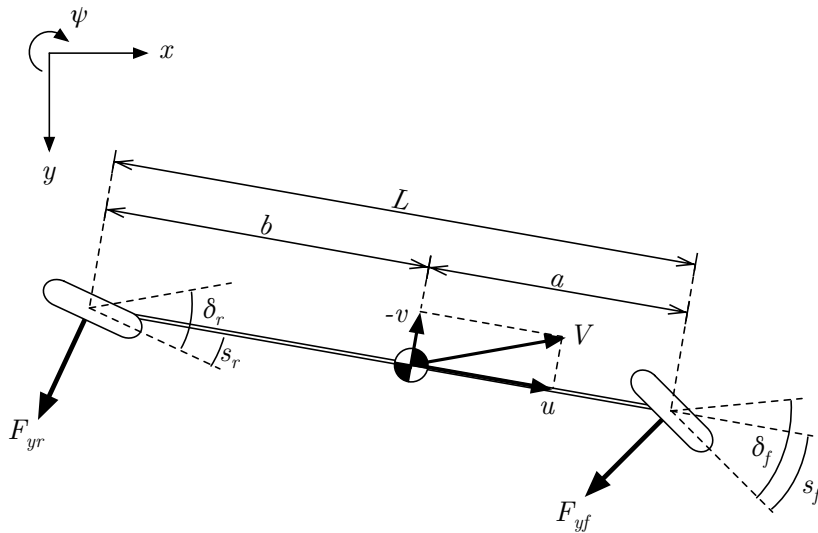


Figure 1: Overview of the Bicycle model.

Several equations are needed to describe a car's motion, in this report the Lagrange method is used to derive the equations of motion.

3.1.1 Lagrange equations

For a system with n degrees of freedom n coordinates q_i are used to describe the motion of the car. Lagrange's equation for coordinate q_i is:

$$\frac{d}{dt} \frac{\partial T}{\partial \dot{q}_i} - \frac{\partial T}{\partial q_i} + \frac{\partial U}{\partial q_i} = Q_i \quad (1)$$

with kinetic energy T , potential energy U , non-conservative forces Q_i and generalized coordinates q_i . By using Lagrange's equation (1) the equation of motion expressed in the coordinates x , y and yaw angle ψ with respect to the global system can be derived, see figure 1. But the expressions are desired to be in the local frame of the car expressed in u , v and ψ instead. Therefore some modifications of the Lagrange equation are needed [3]. The relationship for the variables is:

$$\begin{aligned} u &= \dot{x} \cos \psi + \dot{y} \sin \psi \\ v &= -\dot{x} \sin \psi + \dot{y} \cos \psi \end{aligned} \quad (2)$$

Preparation of the second term in the Lagrange equation (1) yields:

$$\begin{aligned} \frac{\partial T}{\partial x} &= \frac{\partial T}{\partial u} \frac{\partial u}{\partial x} + \frac{\partial T}{\partial v} \frac{\partial v}{\partial x} \\ \frac{\partial T}{\partial y} &= \frac{\partial T}{\partial u} \frac{\partial u}{\partial y} + \frac{\partial T}{\partial v} \frac{\partial v}{\partial y} \\ \frac{\partial T}{\partial \psi} &= \frac{\partial T}{\partial u} \frac{\partial u}{\partial \psi} + \frac{\partial T}{\partial v} \frac{\partial v}{\partial \psi} \end{aligned} \quad (3)$$

By using the expressions for u and v from equation (2) we obtain:

$$\frac{\partial u}{\partial x} = \frac{\partial u}{\partial y} = \frac{\partial v}{\partial x} = \frac{\partial v}{\partial y} = 0 \quad (4)$$

$$\frac{\partial u}{\partial \psi} = -\dot{x} \sin \psi + \dot{y} \cos \psi = v \quad (5)$$

$$\frac{\partial v}{\partial \psi} = -\dot{x} \cos \psi - \dot{y} \sin \psi = -u \quad (6)$$

Substituting equations (4), (5) and (6) into (3) results in:

$$\begin{aligned} \frac{\partial T}{\partial x} &= 0 \\ \frac{\partial T}{\partial y} &= 0 \\ \frac{\partial T}{\partial \psi} &= \frac{\partial T}{\partial u} v - \frac{\partial T}{\partial v} u \end{aligned} \quad (7)$$

Using equation (2) the relationship between u , v and x , y becomes:

$$\begin{bmatrix} u \\ v \end{bmatrix} = R \begin{bmatrix} \dot{x} \\ \dot{y} \end{bmatrix} \iff \begin{bmatrix} \dot{x} \\ \dot{y} \end{bmatrix} = R^{-1} \begin{bmatrix} u \\ v \end{bmatrix} \quad (8)$$

with

$$R = \begin{bmatrix} \cos \psi & \sin \psi \\ -\sin \psi & \cos \psi \end{bmatrix} \quad (9)$$

Using equation (2) preparation of the first term of the Lagrange equation (1) for u and v yields:

$$\frac{\partial T}{\partial \dot{x}} = \frac{\partial T}{\partial u} \frac{\partial u}{\partial \dot{x}} + \frac{\partial T}{\partial v} \frac{\partial v}{\partial \dot{x}} = \frac{\partial T}{\partial u} \cos \psi - \frac{\partial T}{\partial v} \sin \psi \quad (10)$$

$$\frac{\partial T}{\partial \dot{y}} = \frac{\partial T}{\partial u} \frac{\partial u}{\partial \dot{y}} + \frac{\partial T}{\partial v} \frac{\partial v}{\partial \dot{y}} = \frac{\partial T}{\partial u} \sin \psi + \frac{\partial T}{\partial v} \cos \psi \quad (11)$$

This results in:

$$\begin{bmatrix} \frac{\partial T}{\partial \dot{x}} \\ \frac{\partial T}{\partial \dot{y}} \end{bmatrix} = R^{-1} \begin{bmatrix} \frac{\partial T}{\partial u} \\ \frac{\partial T}{\partial v} \end{bmatrix} \quad (12)$$

Due to the fact that the center of gravity does not move along the z -axis the potential energy, U , is zero. The following set of equations for the variables u and v are obtained:

$$\frac{d}{dt} \begin{bmatrix} \frac{\partial T}{\partial \dot{x}} \\ \frac{\partial T}{\partial \dot{y}} \end{bmatrix} = R^{-1} \frac{d}{dt} \begin{bmatrix} \frac{\partial T}{\partial u} \\ \frac{\partial T}{\partial v} \end{bmatrix} + \frac{d}{dt} R^{-1} \begin{bmatrix} \frac{\partial T}{\partial u} \\ \frac{\partial T}{\partial v} \end{bmatrix} = \begin{bmatrix} Q_x \\ Q_y \end{bmatrix} \quad (13)$$

Calculating the time derivative of R^{-1} :

$$\frac{d}{dt} R^{-1} = \dot{\psi} \begin{bmatrix} -\sin \psi & -\cos \psi \\ \cos \psi & -\sin \psi \end{bmatrix} \quad (14)$$

The non-conservative forces Q_i are now expressed with respect to the global system but it is desired to express them in the local frame. Therefore Q_i needs to be transformed with R :

$$\begin{bmatrix} Q_x \\ Q_y \end{bmatrix} = R^{-1} \begin{bmatrix} Q_u \\ Q_v \end{bmatrix} \quad (15)$$

Substituting equation (14) and (15) into (13):

$$R^{-1} \frac{d}{dt} \begin{bmatrix} \frac{\partial T}{\partial u} \\ \frac{\partial T}{\partial v} \end{bmatrix} + \dot{\psi} \begin{bmatrix} -\sin \psi & -\cos \psi \\ \cos \psi & -\sin \psi \end{bmatrix} \begin{bmatrix} \frac{\partial T}{\partial u} \\ \frac{\partial T}{\partial v} \end{bmatrix} = R^{-1} \begin{bmatrix} Q_u \\ Q_v \end{bmatrix} \quad (16)$$

By multiplying every term with R the R^{-1} can be disregarded because $RR^{-1} = 1$:

$$\begin{aligned} \frac{d}{dt} \begin{bmatrix} \frac{\partial T}{\partial u} \\ \frac{\partial T}{\partial v} \end{bmatrix} + \dot{\psi} R \begin{bmatrix} -\sin \psi & -\cos \psi \\ \cos \psi & -\sin \psi \end{bmatrix} \begin{bmatrix} \frac{\partial T}{\partial u} \\ \frac{\partial T}{\partial v} \end{bmatrix} &= \begin{bmatrix} Q_u \\ Q_v \end{bmatrix} \\ \iff \frac{d}{dt} \begin{bmatrix} \frac{\partial T}{\partial u} \\ \frac{\partial T}{\partial v} \end{bmatrix} + \dot{\psi} \begin{bmatrix} 0 & -1 \\ 1 & 0 \end{bmatrix} \begin{bmatrix} \frac{\partial T}{\partial u} \\ \frac{\partial T}{\partial v} \end{bmatrix} &= \begin{bmatrix} Q_u \\ Q_v \end{bmatrix} \end{aligned} \quad (17)$$

Using equations (1), (7) and (17) the modified Lagrange equations expressed in u , v and ψ can be derived:

$$\begin{aligned} \frac{d}{dt} \frac{\partial T}{\partial u} - \dot{\psi} \frac{\partial T}{\partial v} &= Q_u \\ \frac{d}{dt} \frac{\partial T}{\partial v} + \dot{\psi} \frac{\partial T}{\partial u} &= Q_v \\ \frac{d}{dt} \frac{\partial T}{\partial \psi} - v \frac{\partial T}{\partial u} + u \frac{\partial T}{\partial v} &= Q_{\dot{\psi}} \end{aligned} \quad (18)$$

where

$$T = \frac{mv^2}{2} + \frac{mu^2}{2} + \frac{I\dot{\psi}^2}{2} \quad (19)$$

3.1.2 Nonlinear Bicycle Model and the Magic Formula

A car with large steering angles is nonlinear due to the sinusoidal functions. Therefore the Magic Formula is introduced to describe the nonlinearities in the tires [4] and the sinusoidal functions are not neglected. The Bicycle model is then linearized for usage in the control design.

By the help of figure 1, basic trigonometry and the modified Lagrange equations the equations describing the nonlinear system can be determined:

$$m(\dot{v} + u\dot{\psi}) = F_{yf} \cos(s_f) + F_{yr} \cos(s_r) \quad (20)$$

$$I\ddot{\psi} = aF_{yf} \cos(s_f) - bF_{yr} \cos(s_r) \quad (21)$$

$$\delta_f = s_f - \arctan\left(\frac{v + a\dot{\psi}}{u}\right) \quad (22)$$

$$\delta_r = s_r - \arctan\left(\frac{v - b\dot{\psi}}{u}\right) \quad (23)$$

The Magic Formula is a widely used semi-empirical tire model to calculate tire forces and moment characteristics. The formula is used to estimate the lateral tire forces, F_y . The general form of the formula [4]:

$$y = D \sin \left(C \arctan \left(Bx - E(Bx - \arctan(Bx)) \right) \right) \quad (24)$$

where

y	Output variable (in this case F_y).
x	Input variable (in this case slip angle δ).
B	Stretches the curve and is called the <i>stiffness factor</i> .
C	Determines the part used of the sine therefor influences the shape of the curve, called the <i>shape factor</i> .
D	Called <i>peak value</i> and determines the peak of the characteristic.
E	Used to modify the characteristics around the peak of the curve, called the <i>curvature factor</i> .

The constants B , C , D and E are tire specific i.e. these differ from tire to tire.

Estimating the lateral forces using the Magic Formula gives:

$$F_{yf} = D_f \sin \left(C_f \arctan \left(B_f \tan(\delta_f) - E_f (B_f \tan(\delta_f) - \arctan(B_f \tan(\delta_f))) \right) \right) \quad (25)$$

$$F_{yr} = D_r \sin \left(C_r \arctan \left(B_r \tan(\delta_r) - E_r (B_r \tan(\delta_r) - \arctan(B_r \tan(\delta_r))) \right) \right) \quad (26)$$

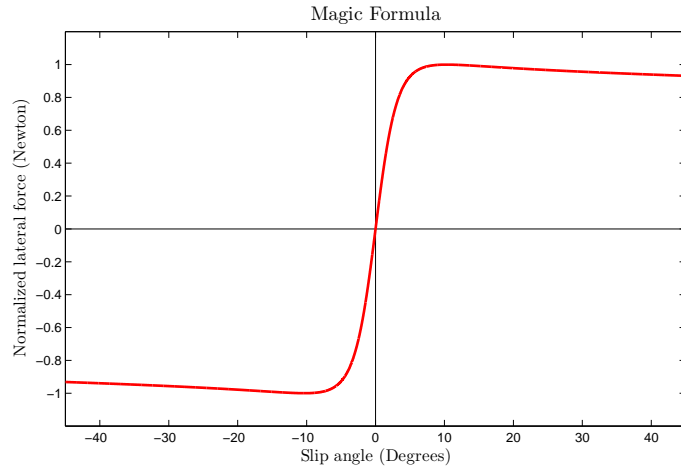


Figure 2: Normalized plot of Magic formula curve.

for only a front steered vehicle, the model is extended with rear wheel steering and also includes the Magic Formula.

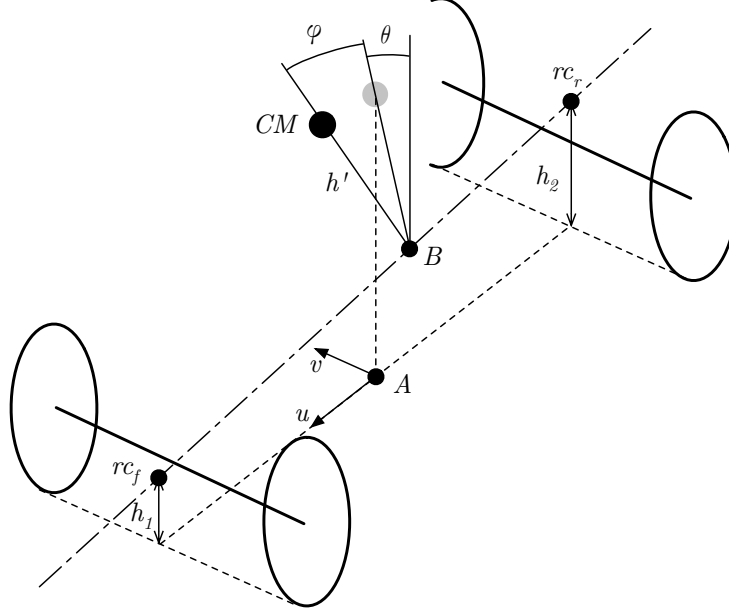


Figure 3: Isometric view of Two Track model.

Several reference frames are introduced to derive the equations of motion:

- e^0 : The global reference frame.
- e^1 : The moving base in point A . This frame is rotated around the z -axis in reference frame e^0 with yaw angle ψ .
- e^2 : The moving base in point B . This frame is rotated around the y -axis in reference frame e^1 with θ , the roll axis inclination angle.
- e^3 : The body fixed frame in point B , e^3 is rotated around the x -axis in reference frame e^2 with the roll angle φ .
- e^4 : The body fixed frame in point CM . This frame is parallel to e^1 when the roll angle is equal to zero. The frame is used to define the inertia matrix.

3.2.1 Lagrange equations

Similar to the Bicycle model (see section 3.1) the equations of motion are derived using Lagrange's equation. The Lagrange expressions for u , v and $\dot{\psi}$, equation (18) remain the same for the Two Track model as for the Bicycle model. It is only the expression for the roll that needs to be augmented. The Lagrange equations becomes:

$$\begin{aligned}
\frac{d}{dt} \frac{\partial T}{\partial u} - \dot{\psi} \frac{\partial T}{\partial v} &= Q_u \\
\frac{d}{dt} \frac{\partial T}{\partial v} + \dot{\psi} \frac{\partial T}{\partial u} &= Q_v \\
\frac{d}{dt} \frac{\partial T}{\partial \dot{\psi}} - v \frac{\partial T}{\partial u} + u \frac{\partial T}{\partial v} &= Q_{\dot{\psi}} \\
\frac{d}{dt} \frac{\partial T}{\partial \dot{\varphi}} - \frac{\partial T}{\partial \varphi} + \frac{\partial U}{\partial \varphi} &= Q_{\varphi}
\end{aligned} \tag{31}$$

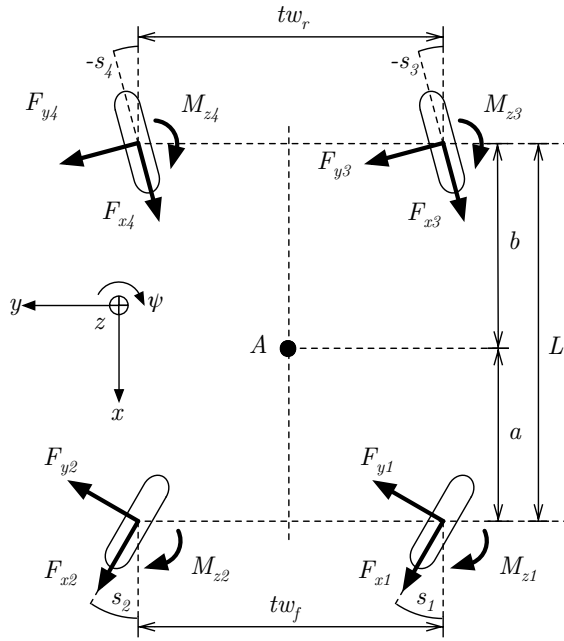


Figure 4: Non-conservative forces, Two Track model.

Figure 4 is a view of the non-conservative forces affecting the car. From this figure the expressions for Q_i can be obtained:

$$\begin{aligned}
Q_u = \sum F_x &= F_{x1} \cos(s_1) + F_{x2} \cos(s_2) + F_{x3} \cos(s_3) + F_{x4} \cos(s_4) \\
&\quad - F_{y1} \sin(s_1) - F_{y2} \sin(s_2) - F_{y3} \sin(s_3) - F_{y4} \sin(s_4)
\end{aligned} \tag{32}$$

$$\begin{aligned}
Q_v = \sum F_y &= F_{x1} \sin(s_1) + F_{x2} \sin(s_2) + F_{x3} \sin(s_3) + F_{x4} \sin(s_4) \\
&\quad + F_{y1} \cos(s_1) + F_{y2} \cos(s_2) + F_{y3} \cos(s_3) + F_{y4} \cos(s_4)
\end{aligned} \tag{33}$$

$$\begin{aligned}
Q_{\psi} = \sum M_z = & a(F_{x1} \sin(s_1) + F_{x2} \sin(s_2)) + a(F_{y1} \cos(s_1) \\
& + F_{y2} \cos(s_2)) + M_{z1} + M_{z2} + M_{z3} + M_{z4} \\
& - b(F_{x3} \sin(s_3) + F_{x4} \sin(s_4)) - b(F_{y3} \cos(s_3) \\
& + F_{y4} \cos(s_4)) + \frac{1}{2}tw_f(F_{x1} \cos(s_1) - F_{y1} \sin(s_1)) \quad (34) \\
& - \frac{1}{2}tw_f(F_{x2} \cos(s_2) - F_{y2} \sin(s_2)) + \frac{1}{2}tw_r(F_{x3} \cos(s_3) \\
& - F_{y3} \sin(s_3)) - \frac{1}{2}tw_r(F_{x4} \cos(s_4) - F_{y4} \sin(s_4))
\end{aligned}$$

$$Q_{\varphi} = \sum M_{\varphi} = -(k_{\varphi f} + k_{\varphi r})\dot{\varphi} \quad (35)$$

where $k_{\varphi f}$ and $k_{\varphi r}$ are the roll damping coefficients.

3.2.2 Kinetic energy

To solve the equations of motion (31) the kinetic and potential energies, T and U need to be derived. The kinetic energy can be described by:

$$T = \frac{1}{2}m\dot{r}_{CM}^T \dot{r}_{CM} + \frac{1}{2}\omega^T J_{CM}\omega \quad (36)$$

where \dot{r}_{CM} is the velocity vector of CM and J_{CM} the matrix of inertia of the car. In order to get the velocity vector \dot{r}_{CM} the length vector r_{CM} needs to be differentiated.

$$r_{CM} = r_A + r_{A \rightarrow B} + r_{B \rightarrow CM} \quad (37)$$

where r_A is the position of point A, $r_{A \rightarrow B}$ and $r_{B \rightarrow CM}$ are the length vectors between A→B and B→CM. The derivative of (37) is:

$$\dot{r}_{CM} = \frac{d}{dt}r_A + \frac{d}{dt}r_{A \rightarrow B} + \frac{d}{dt}r_{B \rightarrow CM} \quad (38)$$

Corioli's theorem is used to take the derivative of the length vectors [6]. The theorem is described by:

$$\dot{W}_{xyz} = \frac{dW}{dt} = \dot{W}_{x'y'z'} + \Omega W \quad (39)$$

where W in this case is a length vector which can change in both x, y, z and rotate around these axes. $\dot{W}_{x'y'z'}$ is the time derivative of vector W as seen by the rotation frame. Ω is the angular velocity.

By applying Corioli's theorem (39) on equation (38) the following expressions are derived:

$$\frac{d}{dt}r_A = \begin{bmatrix} u \\ v \\ 0 \end{bmatrix} \quad (40)$$

$$\frac{d}{dt}r_{A \rightarrow B} = \begin{bmatrix} 0 \\ -\dot{\psi}h' \sin(\theta) \\ 0 \end{bmatrix} \quad (41)$$

$$\frac{d}{dt}r_{B \rightarrow CM} = e^1 \begin{bmatrix} -\sin(\varphi)\dot{\psi}h' - \sin(\theta)\sin(\varphi)h'\dot{\varphi} \\ (\sin(\theta)\dot{\psi} + \dot{\varphi})\cos(\varphi)h' \\ \cos(\theta)\sin(\varphi)\dot{\varphi}h' \end{bmatrix} \quad (42)$$

Equation (40) - (42) in (38) gives:

$$\dot{r}_{CM} = \begin{bmatrix} u - \sin(\varphi)\dot{\psi}h' - \sin(\theta)\sin(\varphi)h'\dot{\varphi} \\ v + h'\sin(\theta)\dot{\psi}(\cos(\varphi) - 1) + \cos(\varphi)h'\dot{\varphi} \\ \cos(\theta)\sin(\varphi)\dot{\varphi}h' \end{bmatrix} \quad (43)$$

The next step is to calculate the second part of the kinetic energy, the inertia. It is assumed that the car is symmetrical with respect to the vertical and longitudinal center plane. This results in both I_{xy} and I_{yz} are equal to zero and $I_{xz} = I_{zx}$. The inertia matrix in reference frame e^4 (position CM) becomes:

$$J_{CM} = \begin{bmatrix} I_x & 0 & -I_{xz} \\ 0 & I_y & 0 \\ -I_{xz} & 0 & I_z \end{bmatrix} \quad (44)$$

The inertia matrix is expressed in reference frame e^4 therefor the angular velocities need to be expressed in this frame as well:

$$\omega = \begin{bmatrix} \cos(\theta)(\sin(\theta)\dot{\psi} + \dot{\varphi}) - \sin(\theta)\cos(\theta)\cos(\varphi)\dot{\psi} \\ \cos(\theta)\sin(\varphi)\dot{\psi} \\ \sin(\theta)(\sin(\theta)\dot{\psi} + \dot{\varphi}) + \cos^2(\theta)\cos(\varphi)\dot{\psi} \end{bmatrix} \quad (45)$$

The equations of motion are complex but several simplifications can be made due to small angles. In \dot{r}_{CM} , (43), and ω , (45), both φ and θ are small therefor are these approximated with second order Taylor expansions. Third and higher-order terms are neglected because of their small impact on the results. The simplification of \dot{r}_{CM} and ω becomes:

$$\dot{r}_{CM} = \begin{bmatrix} u - \varphi\dot{\psi}h' - \theta\dot{\varphi}\varphi h' \\ v + h'\dot{\varphi} - \frac{1}{2}\dot{\varphi}^2 h' \\ \dot{\varphi}h'\varphi \end{bmatrix} \quad (46)$$

$$\omega = \begin{bmatrix} \dot{\varphi} - \frac{1}{2}\theta^2\dot{\varphi} \\ \varphi\dot{\psi} \\ \dot{\varphi}\theta + \dot{\psi} - \frac{1}{2}\varphi^2\dot{\psi} \end{bmatrix} \quad (47)$$

Inserting equations (45) - (47) in (36) gives the total kinetic energy, T , see appendix B equation (75).

3.2.3 Potential energy

There are two components building up the total potential energy: the energy in the torsional springs and the gravitational energy.

$$U = U_s + U_g \quad (48)$$

The torsional spring energy, U_s , is generated by the front and rear roll stiffnesses, $c_{\varphi f}, c_{\varphi r}$. U_s is calculated as a two standard torsional springs:

$$U_s = \frac{1}{2}c_{\varphi f}\varphi^2 + \frac{1}{2}c_{\varphi r}\varphi^2 \quad (49)$$

Note when the roll angle is equal to zero U_s is equal to zero, i.e. no potential energy is built up in the springs.

The gravitational energy, U_g , is defined as zero when the roll angle is zero. Thus U_g is defined as:

$$U_g = mgh'(\cos(\varphi)\cos(\theta) - \cos(\theta)) \quad (50)$$

Equations (49) and (50) in (48) give the total potential energy in the system:

$$U = \frac{1}{2}\varphi^2(c_{\varphi f} + c_{\varphi r}) + mgh'(\cos(\varphi)\cos(\theta) - \cos(\theta)) \quad (51)$$

By using Taylor expansion and neglecting higher order terms, U can be simplified to:

$$U = \frac{1}{2}\varphi^2(c_{\varphi f} + c_{\varphi r}) + \frac{1}{2}\varphi^2mgh' \quad (52)$$

3.2.4 Self-aligning torque

The torques $M_{z,i}$ are called the self-aligning torque for wheel i and are created in the tires as they roll along. The torque tends to steer the tire towards the vehicle's traveling direction. The torque depends on the lateral force (F_y), caster angle, pneumatic and mechanical trail. It is expressed according to Milliken and Milliken [7] as:

$$M_{z,i} = (Pneu_i + Mech_i)\cos(Caster_i)F_{y,i} \quad (53)$$

3.2.5 Load transfer

The load transfer distributes the vertical force applied to each tire. The variable $D_{f,r}$ in the Magic Formula, presented in section 3.1.2, depends on the vertical force of the tire. The vertical force depends in turn of the load transfer. In reality load transfer varies with accelerations, yaw and roll motion. To get more dynamics in the Two Track model the load transfer will be included in the model. The function used to model this depends only on yaw and roll motion presented in [8]. The equations are presented below in equations (54) and (55).

$$F_{z,right} = \left(m(-h'\ddot{\varphi}\sin(\varphi) - h'\dot{\varphi}^2\cos(\varphi) + g - \frac{(c_{\varphi f} + c_{\varphi r})\varphi + (k_{\varphi f} + k_{\varphi r})\dot{\varphi}}{mh}\sin(\varphi)) - \frac{\frac{4}{(tw_f + tw_r)}(I_{xx}\ddot{\varphi} + (I_{zz} - I_{yy})(\dot{\psi}^2\cos(\varphi)\sin(\varphi)))}{1 + \frac{4}{(tw_f + tw_r)}h'\sin(\varphi)} \right) // \quad (54)$$

$$\left(1 - \left(\frac{\frac{4}{(tw_f + tw_r)}h'\sin(\varphi) - 1}{\frac{4}{(tw_f + tw_r)}h'\sin(\varphi) + 1} \right) \right)$$

$$F_{z,left} = \frac{4}{(tw_f + tw_r)} \left(I_{xx}\ddot{\varphi} + (I_{zz} - I_{yy})(\dot{\psi}^2\cos(\varphi)\sin(\varphi) - h'\sin(\varphi))F_{z,right} + F_{z,right} \right) // \left(1 + \frac{4}{(tw_f + tw_r)}h'\sin(\varphi) \right) \quad (55)$$

The car is assumed to be symmetrical w.r.t. the u, z -plane, but not to the v, z -plane. Because of that the load transfer is not the same on both the tires on the left or right side. It is going to be distributed according to the weight distribution of the car, see equation (56). The car is assumed to have an equal weight distribution, like a solid block.

$$\begin{aligned} F_{z,1} &= F_{z,left} \left(\frac{a}{a+b} \right) \\ F_{z,2} &= F_{z,right} \left(\frac{a}{a+b} \right) \\ F_{z,3} &= F_{z,left} \left(\frac{b}{a+b} \right) \\ F_{z,4} &= F_{z,right} \left(\frac{b}{a+b} \right) \end{aligned} \quad (56)$$

3.2.6 Final state equations

All the segments for deriving the final state equations of motion are now available. In order to be able to substitute every part in equation (31) the partial derivatives of T and U with respect to the states need to be calculated, as well as the time derivative of these. The needed partial and time derivatives are found in appendix B.2, equations (76) - (84).

Substituting equations (32) - (35), (76) - (84) in (31) and then isolate the state derivatives gives the final state equations. The final state equations are found in appendix B.3 equations (85) - (88).

4 Control design

There are three different derived ways to control the rear wheels; one for low speed, one for high speed and one for the parallel parking. The control designs are described in the upcoming three sections.

4.1 Low speed

Better maneuverability is desired in low speed ($< 10 \text{ km/h}$). Due to the fact that the car's motion is in principle geometrical in low speeds the chosen controller is a proportional gain (K_p). The steer angle of the front wheels is the input to the controller and the desired rear steering angle the output.

4.2 High speed stability

Stability is the main goal in higher speeds above 70 km/h . In higher speeds the nonlinearities are more significant compared to the lower speeds. In this case an LQ-controller is chosen because of its flexibility to add and remove states that are desired to control.

The states that are used for control, in this application, are the yaw rate ($\dot{\psi}$), yaw (ψ) and lateral velocity (v). These states are chosen because they highly affect the behavior of the car and ARS has a large impact on them. The control principle is illustrated in figure 5.

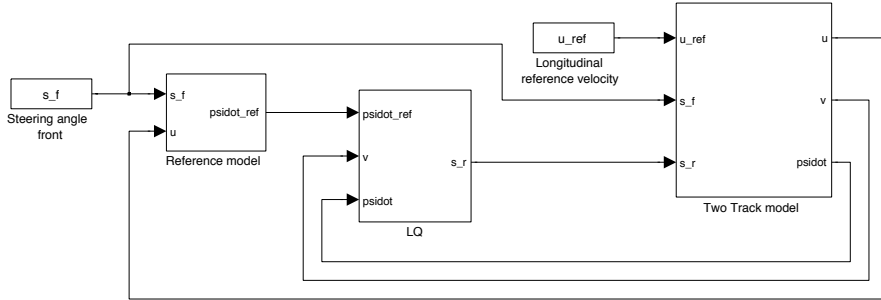


Figure 5: High speed control principle.

A reference model describing the wanted yaw rate is needed. A first order system is used as a reference model [5] to get the appropriate yaw rate with front wheel angle (s_f) and longitudinal velocity (u) as inputs:

$$\dot{\psi}_{ref} = \frac{H_0}{\tau s + 1} s_f \quad (57)$$

where H_0 is:

$$H_0 = \frac{u}{a + b + \frac{\eta}{g}u^2} \quad (58)$$

and η is the understeer coefficient defined by:

$$\eta = \frac{mg}{a + b} \left(\frac{b}{C_{stiff_f}} - \frac{a}{C_{stiff_r}} \right) \quad (59)$$

where C_{stiff_f} and C_{stiff_r} are the cornering stiffnesses front and rear defined by:

$$\begin{aligned} C_{stiff_f} &= B_f C_f D_f * 2\mu \\ C_{stiff_r} &= B_r C_r D_r * 2\mu \end{aligned} \quad (60)$$

with time constant τ as:

$$\tau = \frac{I}{aC_f} H_0 \quad (61)$$

A first order system gives a smooth transition between yaw rates and suppresses overshoots, which gives the wanted behavior of the car.

A linear model needs to be derived to be able to use LQ. The derived Bicycle model is linearized, see appendix A, extended with an integral state (ψ) and used in the controller. The integral state is used to minimize the steady state error. The LQ-controller is derived using the MATLAB command *lqr* and the Q and R matrices are chosen with the help of Bryson's rule [9] as a guide.

To speed up the system a feedforward gain (K_{ff}) is implemented to reduce the impact of the slow pole introduced by the integral state [10].

4.3 Parallel parking algorithm

Several car manufacturers, such as Volkswagen and Toyota, have today autonomous parallel parking systems but none of them utilizes rear wheel steering.

Research studies have been carried out on a car-like vehicle using fuzzy logic controllers in combination with range sensors to localize, map-learning and parking [11], [12]. Another popular approach is to localize the desired end position and use a chained form with sinusoidal or polynomial inputs [13], [14]. Laugier and Paromtchik suggested in [2] a parallel parking algorithm divided into three steps; max steer in one direction, a sinusoidal steer function and max steer in opposite direction w.r.t. the first step.

The algorithm suggested by Laugier and Paromtchik is going to be used as a basis for this research. The algorithm is modified to utilize rear wheel steering.

4.3.1 Algorithm

The algorithm is built up by three steps in order to get a smooth motion path; maximum steer right, maximum steer left and a sinusoidal transition period between these extreme values, see figure 6. First the car steers at maximum right until time t' , then the transition period T^* uses sinusoidal function as steering input. At last a maximum turn left equally long as the maximum right. T is the total time of the procedure.

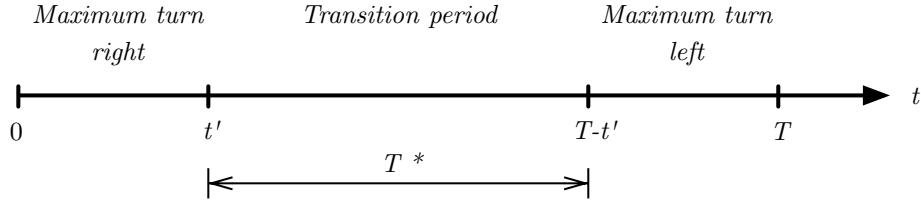


Figure 6: Time axis over parallel parking algorithm.

The output from the algorithm are proposed control signals for the vehicle to parallel park without any collisions. The generated route from the control signals is illustrated in figure 7.

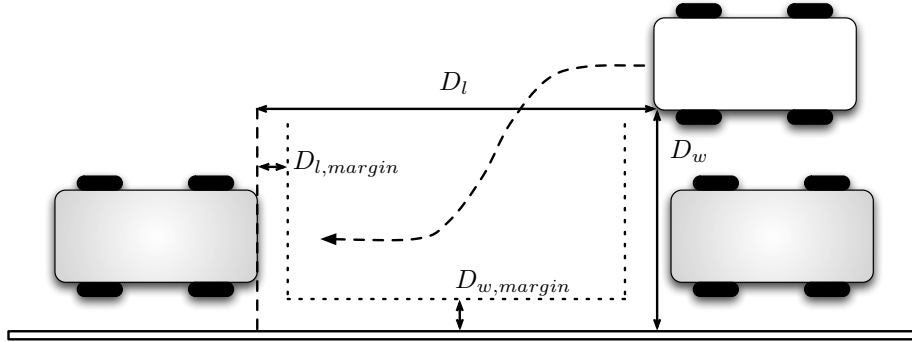


Figure 7: Illustration of a route generated from the control signals.

The algorithm is iterative and needs to estimate the vehicle's end position in order to determine if the desired destination is met. A kinematic model of a four wheel steered car derived by Wang and Qi [15] is used for this matter. The kinematic model is expressed in equations (62) - (64).

$$\dot{x} = \frac{u}{\cos(\beta)} \cos(\psi + \beta) \quad (62)$$

$$\dot{y} = \frac{u}{\cos(\beta)} \sin(\psi + \beta) \quad (63)$$

where

$$\beta = \arctan\left(\frac{a \tan(s_f) + b \tan(s_r)}{a + b}\right) \quad (64)$$

The control signals s_f , s_r and u are calculated from equations (65) and (66). $A(t)$ and $B(t)$ are the sinusoidal functions and are calculated in equations (67) and (68). s_f and s_r are calculated in the same way but with different parameter. Equations (65) and (67) are generic.

$$s(t) = s_{max}A(t) \quad 0 \leq t \leq T \quad (65)$$

$$u(t) = -u_{max}B(t) \quad 0 \leq t \leq T \quad (66)$$

$$A(t) = \begin{cases} 1 & 0 \leq t \\ \cos\left(\frac{\pi(t-t')}{T^*}\right) & t' \leq t \leq T - t' \\ -1 & T - t' \leq t \leq T \end{cases} \quad (67)$$

$$B(t) = 0.5 \left(1 - \cos\left(\frac{4\pi t}{T}\right)\right) \quad (68)$$

where $T^* < T$ and $t' = \frac{T-T^*}{2}$.

T^* , s_{max} and u_{max} are chosen empirically depending on the car and the desired smoothness of the motion. An example of calculated control signals are illustrated in figure 8.

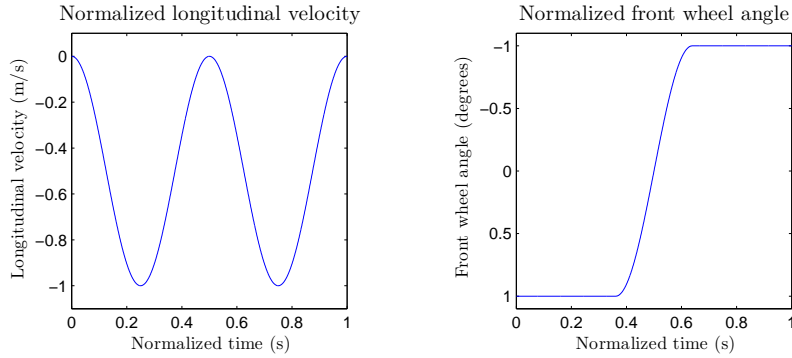


Figure 8: Example of calculated control signals from the parking algorithm.

The algorithm is, as mentioned earlier, iterative and tries to reach the desired end position by changing the variables T and s_{max} . In general you can say that T determines the longitudinal travel and s_{max} the lateral. The lateral position

is harder to reach than the longitudinal and may not be reached. Therefore an outer loop may be needed to repeat the algorithm.

The algorithm is also extended with “crabbing”. Crabbing is when both front and rear wheels have equal steering angle when driving forward or in reverse. This results in a linear motion with both longitudinal and lateral displacement. Crabbing can thereby only be used if the rear wheels can be steered. The car will crab instead of driving in a sinusoidal motion if it will get closer to the end position.

The iteration process stops when the path closest to the end point is found that fulfills the conditions (69) and (70).

$$|x_T \cos(\psi_T) + y_T \sin(\psi_T)| < D_l - D_{l,margin} - overhang_{rear} \quad (69)$$

$$|-x_T \sin(\psi_T) + y_T \cos(\psi_T)| < D_w - D_{w,margin} - \frac{tw_r}{2} \quad (70)$$

where x_T , y_T and ψ_T are the reached end coordinates and angle of car. D_l and D_w are the available parking space illustrated in figure 7. $D_{l,margin}$ and $D_{w,margin}$ are the margins from the parked cars and the wall, i.e. the space where the car is not allowed to be due to safety reasons. $overhang_{rear}$ is the length from rear axle to the rear end of the car.

5 Simulations

In this chapter the results from the different low- and high-speed driving cases, seen in table 1, are presented. These cases are divided into subsections 5.2.1 - 5.3.3. In these subsections the simulated driving cases are described more in detail and which parameters that are changed. The parallel parking algorithm's results are presented in subsection 5.4.

In the simulations a vehicle without ARS was compared with one that has ARS implemented. The maximum rear steer angle was varied during the simulations. In low speeds $< 10 \text{ km/h}$ the ratio between front and rear steer angle was determined by a P-controller (K_p). An LQ-controller was used to stabilize the car and reduce skid in high speed.

5.1 Model validation

The goal of the validation was to assure that the Two Track model was accurate enough to create a controller for the rear wheel steering that could be used as a guideline for implementation in a real car.

The Bicycle model was not used as a simulation model for the car, it was only used as a linear model in the LQ-controller (see section 4.2) therefor it was left out in the validation process.

The Two Track was validated against a VI-CarRealTime model describing a Volvo car. The rear angle in the Two Track model was set to 0 because that the VI-CarRealTime model does not have ARS implemented. The two driving cases that were carried out were "sine 0.5 Hz" (see C.8) and "sine with dwell" (see C.9).

The validation results were satisfying and the model could handle the nonlinearities good enough to be used as a simulation model.

5.1.1 Sine 0.5 Hz

The driving case was simulated with the velocities 30, 80 and 130 km/h and the results are shown in figures 9 - 12.

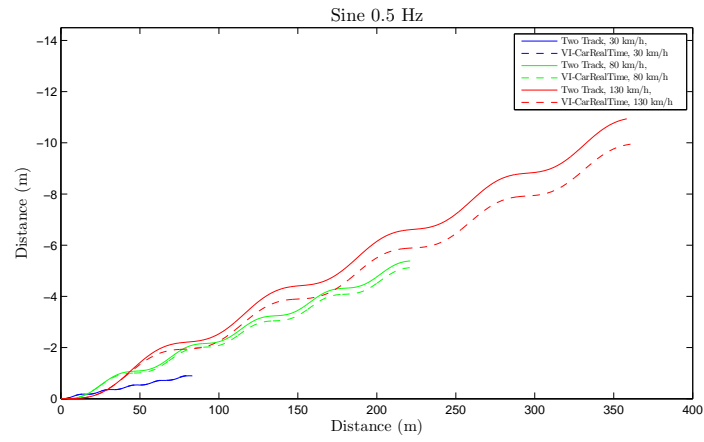


Figure 9: Position of car.

Notice that the scales of the axes are not equal to each other in figure 9. For the simulations run in 30 and 80 km/h the position coincided quite good. For 130 km/h the end position of the Two Track model differed with -2.5 m in longitudinal and 1.0 m in lateral displacement.

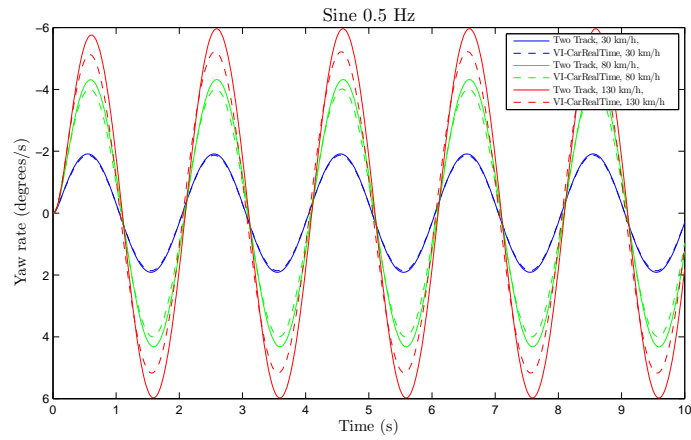


Figure 10: Yaw rate of car.

For 30 km/h the yaw rate coincided. In the higher velocities the difference was small enough to be neglected.

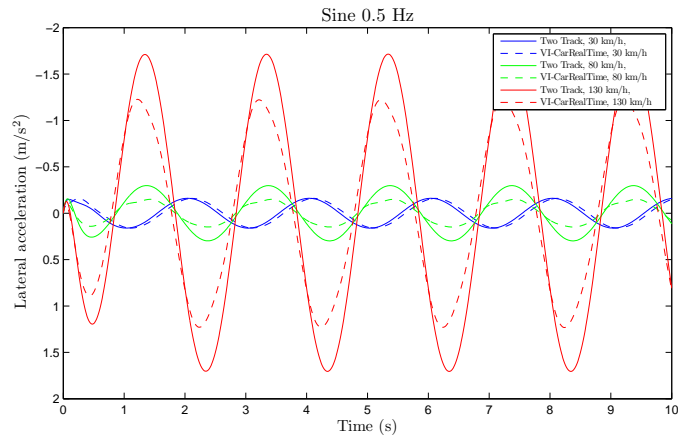


Figure 11: Lateral acceleration of car.

The lateral accelerations in figure 11 differed a bit in the speeds over 30 km/h . This may be a result from the simpler tire model used in the Two Track model compared to the VI-CarRealTime model. The tire model implemented in the Two Track model only estimates the lateral force (F_y) and does not take the longitudinal forces into account. This may also be caused by other simplifications in the model, but this has not been investigated any further.

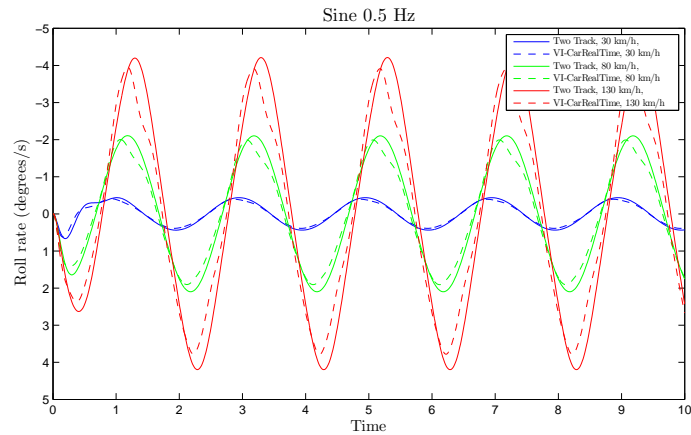


Figure 12: Roll rate of car.

The roll rate had the same behavior as both the yaw rate and the lateral acceleration. Overall the Two Track model performed well in this driving case. For the low speed simulations the model almost coincided with the VI-CarRealTime model.

5.1.2 Sine with dwell

In this driving case, described in appendix C.9, the initial speed was 80 km/h and the amplitude of steering wheel angle was varied. The results are presented in figures 13 - 16. To not clutter the plots of the results only two situations are presented; one with low and one with high amplitude on the steering wheel angle.

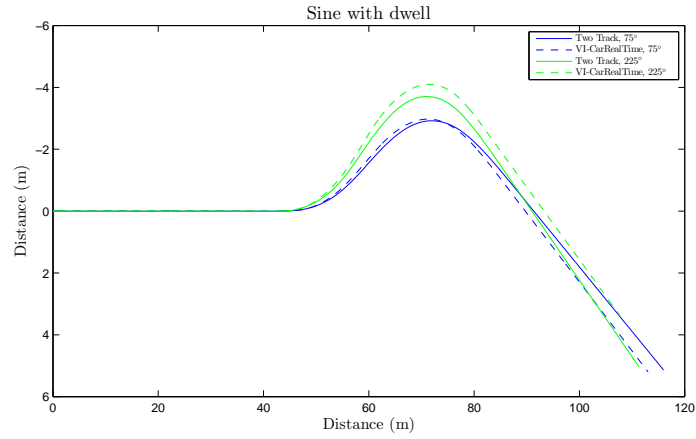


Figure 13: Position of car.

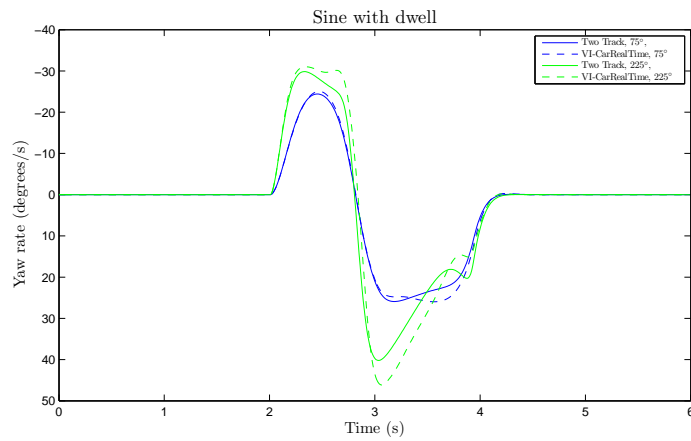


Figure 14: Yaw rate of car.

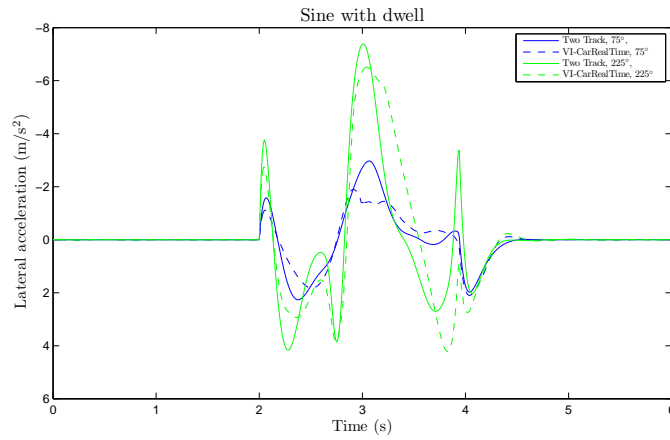


Figure 15: Lateral acceleration of car.

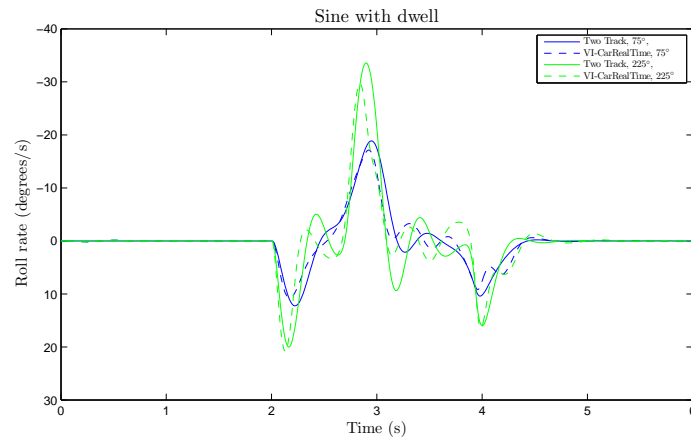


Figure 16: Roll rate of car.

Sine with dwell was chosen to test the nonlinearities in the model to see how well it could handle them. Both position and yaw rate correlated well with simulation results from VI-CarRealTime. Comparing lateral acceleration and roll rate with VI-CarRealTime one can see that they differ but still has the overall same shape.

5.2 Low speed simulations

In the low speed simulations the rate of change of the actuator and time delays were neglected because their impact in low speed were minor compared to high speed. The maximum rear wheel angle was changed from 0° to 2° , 5° and 10° to see how large the impact will be.

5.2.1 Minimum turn radius

The simulations show the minimum turn radius for different maximum rear wheel angles. The car had a reference longitudinal speed of 5 km/h and maximum wheel angle on both the front and rear wheels in off-phase. The results from the simulations can be seen in figure 17 and table 2. The minimum turn radius was defined from outermost wheel.

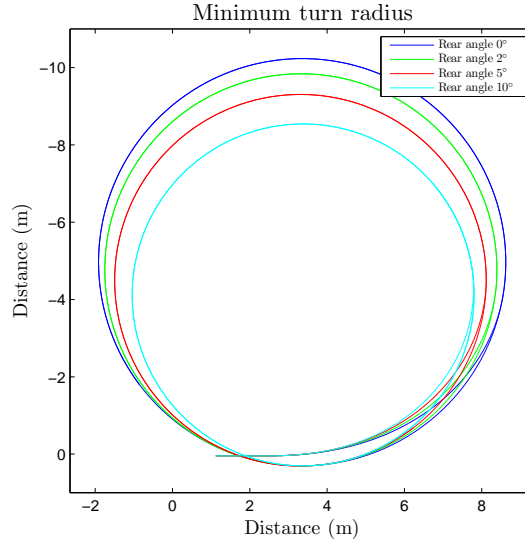


Figure 17: Position of outermost wheel, minimum turn radius.

s_r^{max} ($^\circ$)	Turn radius (m)	Δ Turn radius (m)
0	5.12	-
2	4.92	-0.20
5	4.65	-0.47
10	4.27	-0.85

Table 2: Minimum turn radius results.

As seen in figure 17 and table 2 the turn radius was clearly reduced as one could expect.

5.2.2 S-curve

In this case the angle on the front wheels were varied, from maximum steer left to maximum right, and velocity was kept at 5 km/h which builds up a path that was an S-curve. The ratio between front and rear wheel angles was kept at

-1.0, meaning the same angle until saturation but in off-phase. The simulation was repeated with the same input but with varied maximum rear wheel angle. The front wheel angle over time is illustrated in C.2 figure 38. The results are presented in figure 18 and table 3.

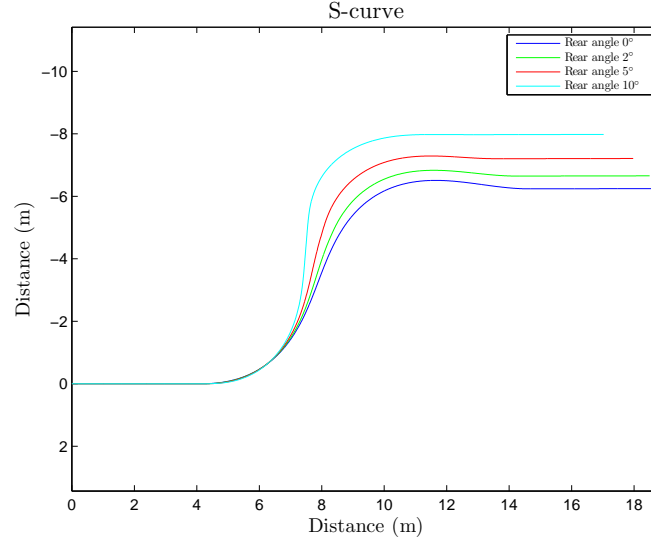


Figure 18: Position of car in S-curve.

s_r^{max} (°)	Lateral displacement (m)	Δ Lateral displacement (m)
0	6.51	-
2	6.83	0.32
5	7.29	0.78
10	7.98	1.47

Table 3: S-curve lateral displacement.

From figure 18 we can see that the turn became tighter and tighter when the maximum rear wheel angle was increased. Thereby the lateral displacement was affected as well. In table 3 we can see that the lateral displacement also became longer as the rear wheel angle was increased.

5.2.3 Follow S-curve

This case was similar to the “S-curve” driving case (section 5.2.2) but here a predefined path of an S-curve was followed, almost identical to the S-curve produced when ARS was deactivated in section 5.2.2. The velocity was held constant at 5 km/h. The front steer angles were controlled via a PD-controller

and the ratio between front and rear wheel angles was kept to -0.5 . The results show the difference in steer angles needed to keep the car on the path, figures 19, 20 and table 4.

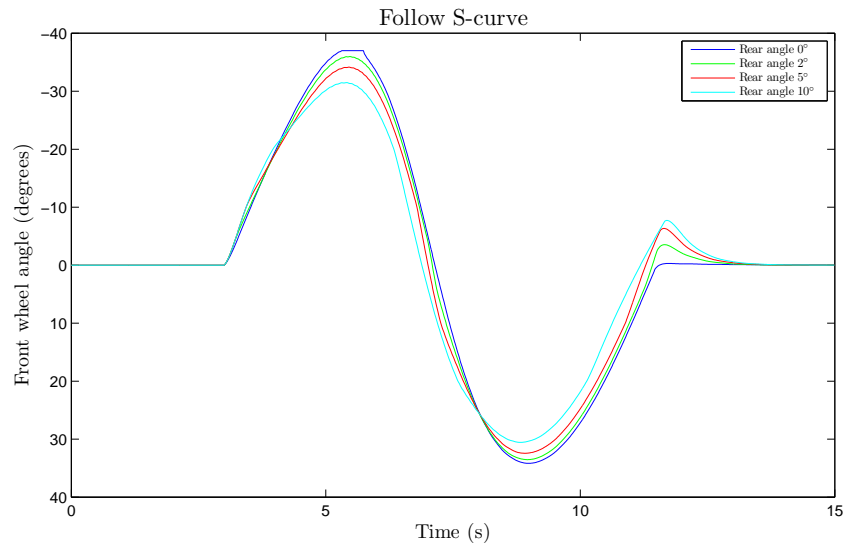


Figure 19: Front wheel angles.

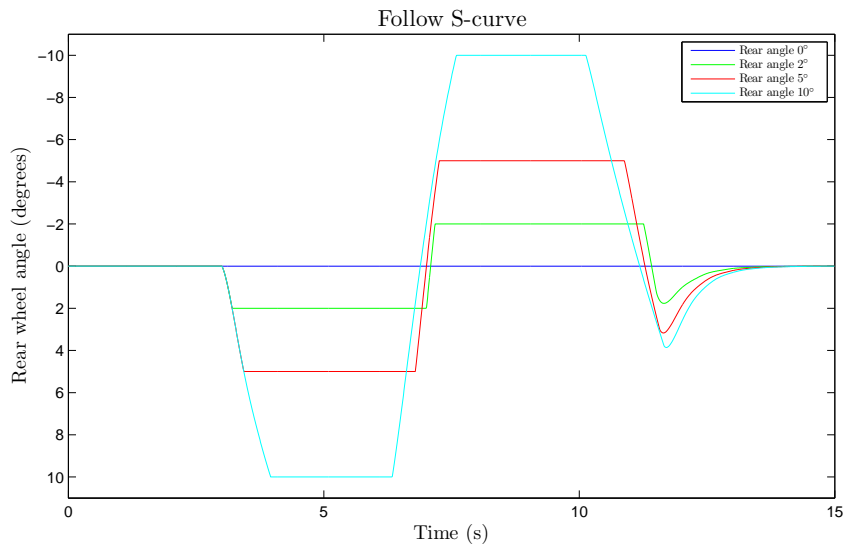


Figure 20: Rear wheel angles.

s_r^{max} ($^\circ$)	$max(s_f)$ ($^\circ$)	$max(\text{Steering wheel angle})$ ($^\circ$)
0	37.0	545.8
2	35.9	529.5
5	34.2	504.5
10	31.5	464.6

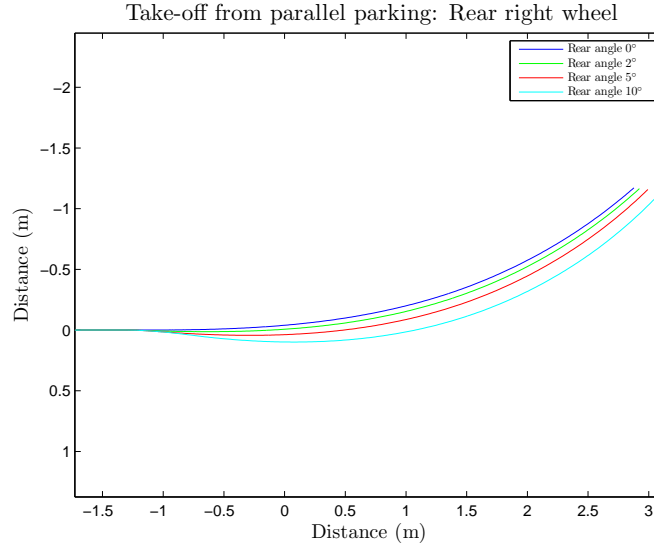
Table 4: Differences in steering wheel angles.

From the simulation results one can see that as the max rear wheel angle increases the maximum needed wheel angle of the front wheel decreases.

5.2.4 Take-off from parallel parking

In this case a simulation of a take-off from a parallel parking spot was performed. It focuses on the car's lateral displacement of the rear end and wheels. This test indicates if there are any potential problems for the wheels colliding with the curb or the car's rear end with the wall when driving from a parallel parking space (see section 1.2 fourth bullet).

The car accelerated up to 5 km/h at the same time the front steer angle was ramped up from 0° to max steer angle in 2 seconds. The maximum rear wheel angle was varied. The car was represented as a rectangle with 1.00 m front and rear overhang from the wheels. The results from the simulations can be found in the figures 21, 22 and tables 5, 6.

**Figure 21:** Lateral displacement of right rear wheel.

s_r^{max} ($^\circ$)	Max lat. displacement (m)	Δ Lateral displacement (m)
0	0.00	-
2	0.01	0.01
5	0.04	0.04
10	0.10	0.10

Table 5: Lateral displacement of right rear wheel.

From the results in figure 21 and table 5 one can see that when ARS was not active there was no positive lateral displacement at all for the rear wheels. When the ARS was active and the max rear wheel angle increased the positive lateral displacement increased as well. For $s_r^{max} = 2^\circ$ the right rear wheel's maximum displacement was just 1 cm. It was therefore concluded that the risk of colliding with the wheels into the curb was minimal when $s_r^{max} = 2^\circ$. The driver has possibly already collided with it earlier if this occurs.

However, when the $s_r^{max} \geq 5^\circ$ the displacement became more noticeable and will probably become a problem that needs to be taken care of in order to avoid collision.

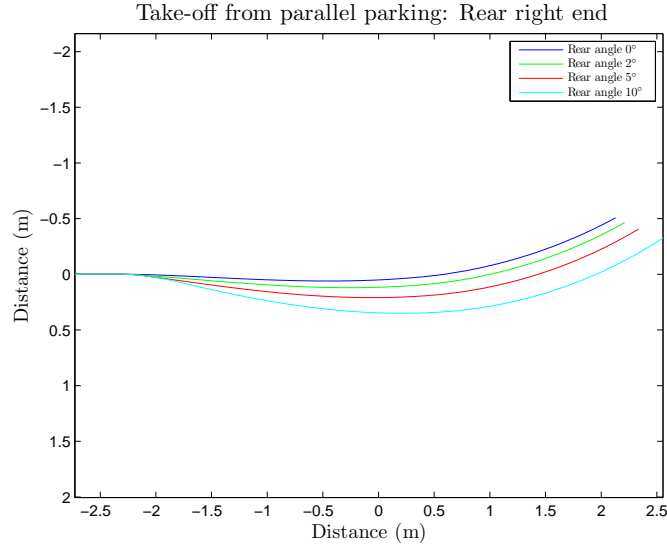


Figure 22: Lateral displacement of right rear end.

s_r^{max} ($^\circ$)	Max lat. displacement (m)	Δ Lateral displacement (m)
0	0.06	-
2	0.12	0.06
5	0.21	0.15
10	0.35	0.29

Table 6: Lateral displacement of right rear end.

The lateral displacement of the car's right rear end when $s_r^{max} = 2^\circ$ was twice as much w.r.t. a car with no ARS. Still, as for the wheels, the risks of colliding with an obstacle is small. But as s_r^{max} increases, above 5° , the risk cannot be neglected anymore and the problem needs to be considered.

For a complete figure of the car's motion for all its corners see appendix D.1.

5.3 High speed simulations

In the high speed simulations described in this section the main goal was to make the car more stable and minimize overshoots and skid compared to a car without ARS. In every subsection the car was simulated both with and without ARS. The rear wheels were controlled via the control principle described in section 4.2.

The LQ-controller needs to be designed around a velocity and friction coefficient. 100 km/h was chosen to investigate if only one controller could handle large regions of the high-speed span. μ was chosen to 0.95 which is a high friction coefficient representing dry asphalt. The Q-matrix was chosen with Bryson's rule [9] as base and was tuned such that the controller could handle system delays (sensor readings, actuator, bus) up to 120 ms .

During the simulations it was discovered that the reference model had a large impact to the system and its output. It was important to verify that the reference model was fine-tuned to get desirable results. This is further described in the upcoming section 5.3.1.

5.3.1 Step steer

In these simulations the responsiveness and skid of the car were studied when doing a quick turn. The front wheel angle was ramped from 0° to -1.5° in 0.4 seconds and then held constant. The velocity was held constant at 100 km/h during the whole simulation. The rear wheels were controlled by the LQ-controller and μ was set to 0.95. Delays were included in the actuator and sensor readings in the Two Track model to better model the reality.

As mentioned earlier the reference model had a large impact to the system. The gain and the time constant in the model needed to be fine-tuned. The gain also needed to be constrained due to the fact that the reference model was linear

and the Two Track model was not. The step steer driving case was suitable as test for fine-tuning the reference model due to the steady state behavior.

The reference model was fine-tuned and the results of varying the time constant (τ) and gain (H_0) are visualized in figure 23.

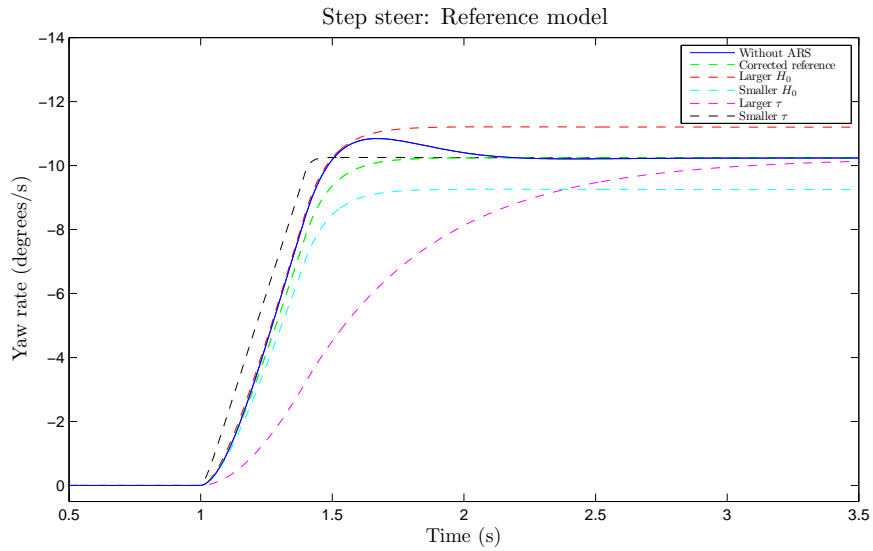


Figure 23: Manipulation of τ and H_0 in the reference model.

The blue line is the Two Track model without ARS. The car reached steady state after 2.5 seconds and it was the desired steady state for the reference model. The unchanged reference model had a higher steady state yaw rate and a bit slow time constant, therefore it was needed to be fine-tuned.

The slow pole introduced by the integral state (see section 4.2) resulted in a slow system response. To deal with this a feedforward gain (K_{ff}) was introduced. The gain calculated was not satisfying and needed to be fine-tuned as well as the reference model. Too much negative K_{ff} made the car skid and the yaw rate got an overshoot. Too much positive K_{ff} gave a slow response. The impact to the system when varying the K_{ff} can be seen in figure 24.

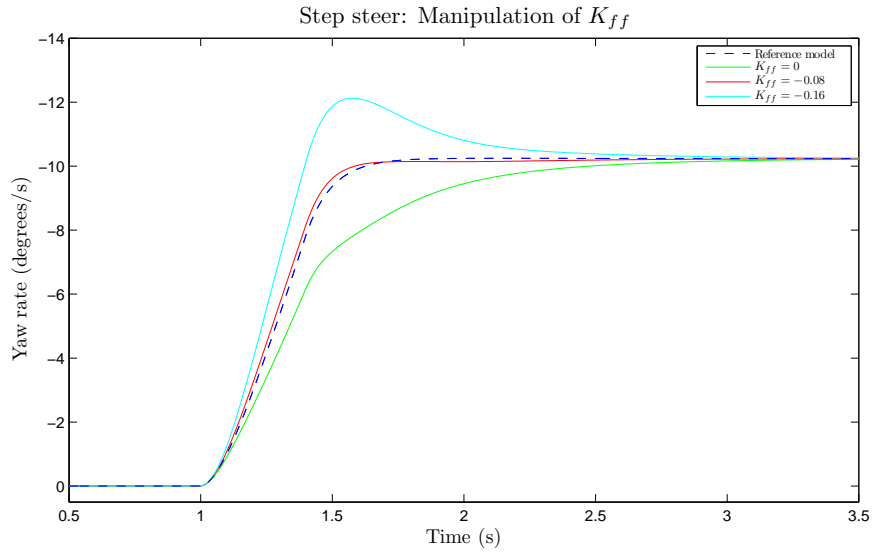


Figure 24: Manipulation of the feedforward gain K_{ff} in the LQ controller.

Even relatively small variations of K_{ff} gave large changes of the car's behavior as seen in the figure above.

When driving on a slippery surface ($\mu < 0.3$) the car tends skid when turning. ARS could potentially stabilize the car in this situation. The controller was put to the test with a μ lower than 0.95. The simulation results are presented in figure 25.

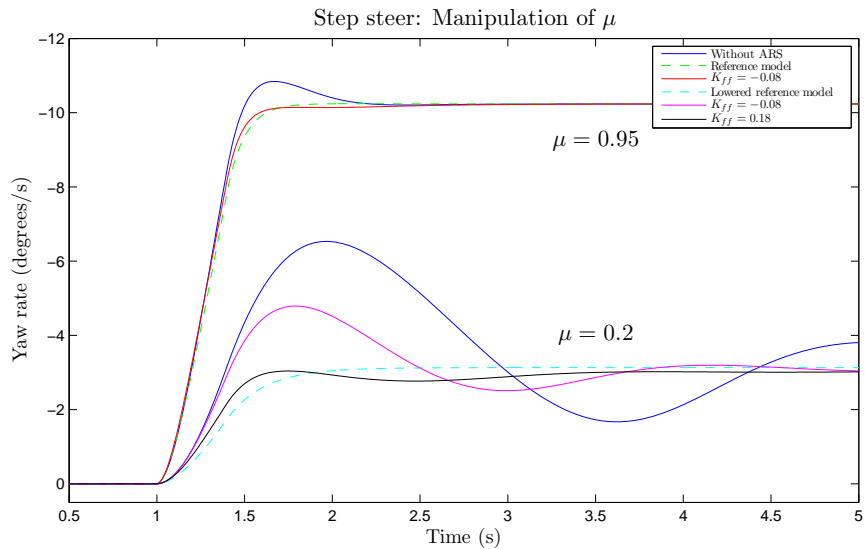


Figure 25: Comparison between non-slippery and slippery surface, $\mu = 0.95$ and $\mu = 0.2$.

The reference model gain was too large when $\mu = 0.2$ and was lowered a bit to better suit the steady state value for the car without ARS. From the picture above one sees that the feedforward gain needs to be depending on the friction coefficient due to the overshoots. After lowering the reference model gain and adjusted K_{ff} the car with ARS became more stable. The wheel angles of the car can be seen in the appendix section E.1 figure 43.

The LQ-controller was designed around a specific velocity, in this case 100 km/h . The step steer driving case was also used to investigate if the controller could handle both lower and higher velocities. If so the need of having multiple controllers in high speed could be reduced. In figure 26 the step steer was simulated in the velocities; 70 , 100 and 130 km/h .

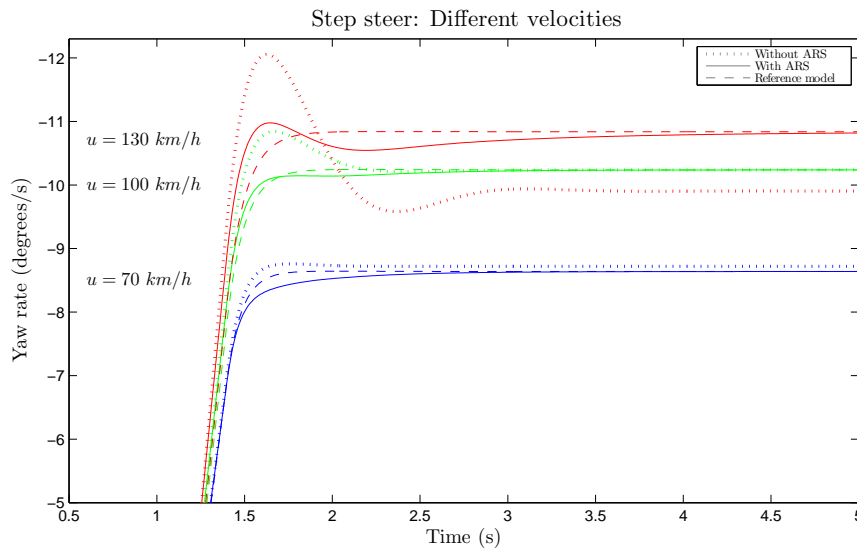


Figure 26: Test of controller in different velocities.

The controller could handle velocities below 100 km/h at a satisfying level, though the system response became a little bit slower. At speeds over 125 km/h the car tended to skid much more than in 100 km/h . As seen in the picture the steady state yaw rate when driving, without ARS, at 130 km/h became lower due to the skid. When the ARS was active the car managed to level out with the yaw rate from the reference model.

5.3.2 Lane change

A more realistic driving case compared to the step steer would be a lane change (see C.6 for more details). A fast lane change on the highway was simulated. The velocity was held constant at 120 km/h . The tuned reference model (see section 5.3.1) was simulated as well as a reference model with higher gain.

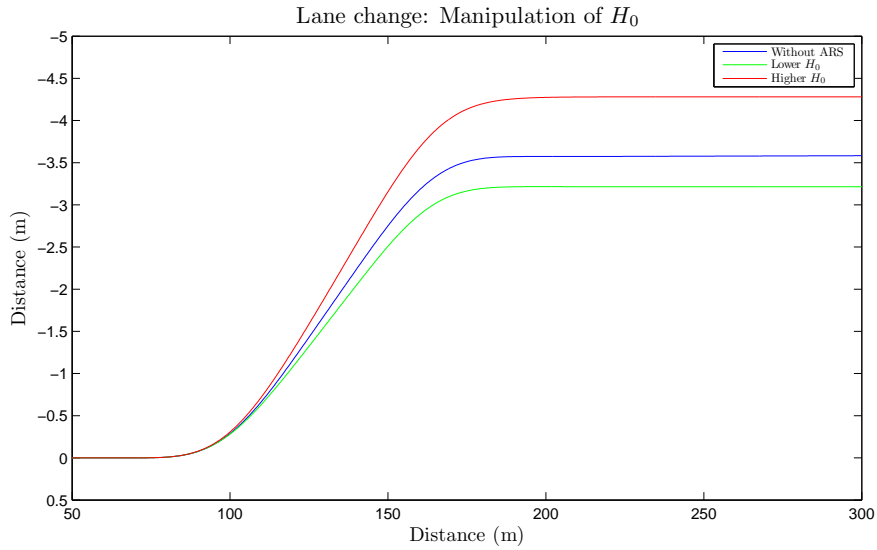


Figure 27: Position of the car using ARS compared to a car without.

When ARS was turned on neither of the end positions matched the one when ARS was turned off, see figure 27. The end position was not the same due to the fact that the reference yaw rate was lower or higher than driving without ARS as seen in figure 28.

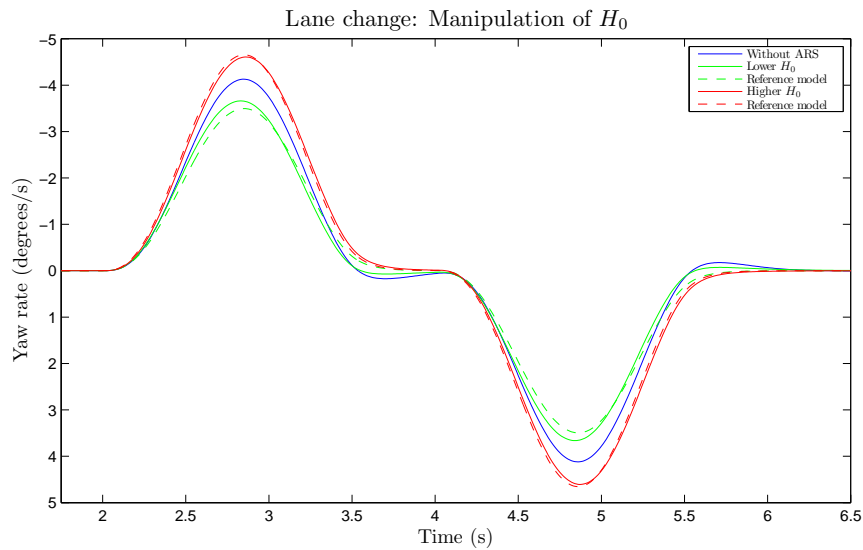


Figure 28: Yaw rate of the car.

When the ARS was turned on the yaw rate overshoots were minimized, thereby the skid, compared to when it was turned off.

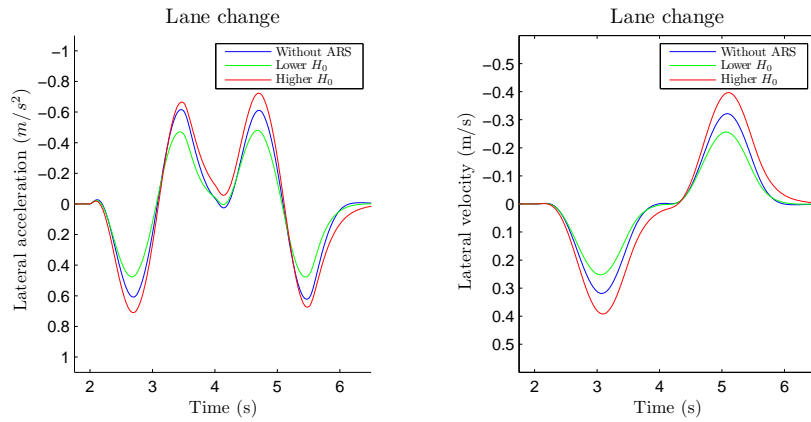


Figure 29: Lane change lateral acceleration.

As one can expect the lateral velocities and accelerations followed the same pattern as the yaw rate; when the reference model had higher gain the lateral accelerations and velocities got higher and vice versa.

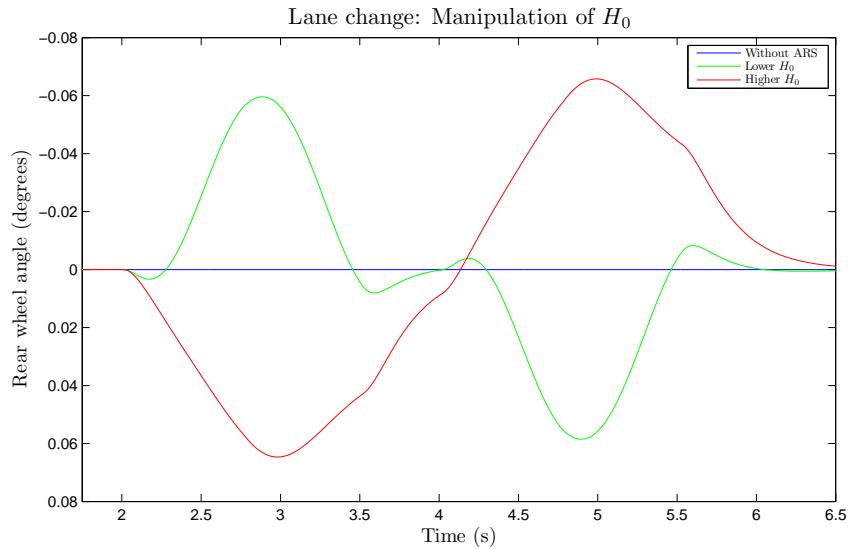


Figure 30: Rear wheel angles for lane change.

Depending on the reference model the car will steer in- or off-phase with the rear wheels. If the reference yaw rate was smaller compared to the yaw rate when the ARS was inactive the wheels will steer in-phase and vice versa as seen in figure 30. If the reference yaw rate would coincide then the rear wheels would only be moving to prevent skid in this case at the times; 3.5 and 5.5.

This shows again that the reference model played a large role of the behavior of the car when implementing ARS.

5.3.3 External lateral force

An external force in lateral direction was applied to the car meanwhile driving straight forward at constant velocity, 100 km/h . It can be seen as a car on the highway driving on a straight road into a strong wind of gust coming from the side. The force applied to the car (distributed equally on the four wheels) was sinus-shaped and illustrated in appendix C.7 figure 40. The results with and without ARS can be seen in figure 31 and 32.

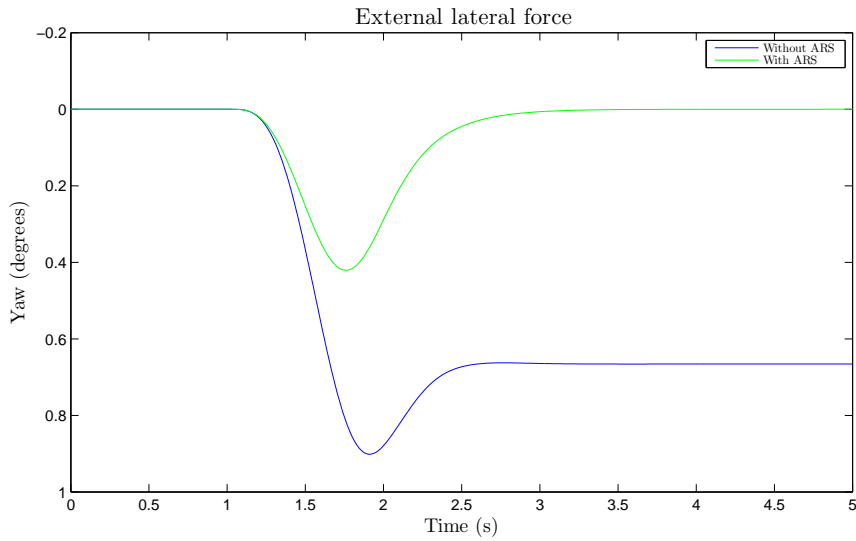


Figure 31: Yaw of the car with and without ARS.

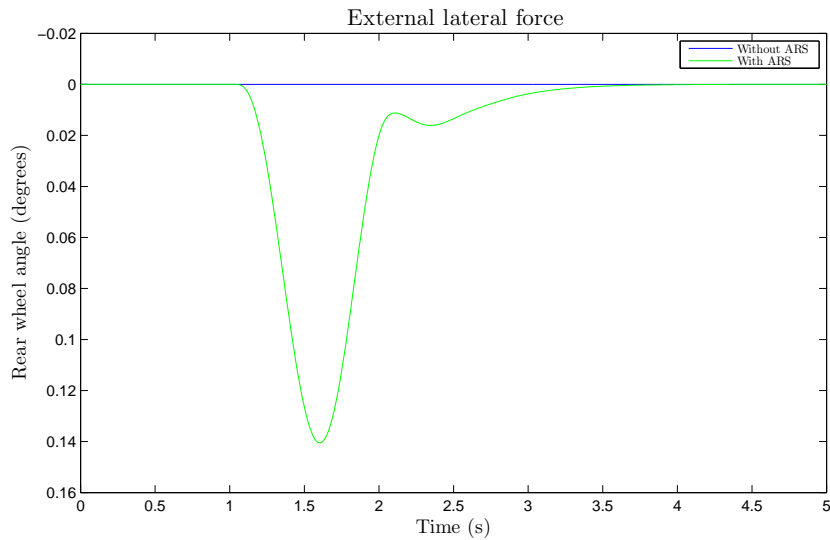


Figure 32: Rear wheel angles.

As seen in the figures the ARS compensates for the external force by steering the rear wheels. The car returns to its original trajectory while without ARS the driver has to compensate for this.

5.4 Parallel parking algorithm

The parking algorithm introduced in section 4.3 was built up and simulated using MATLAB and Simulink. The desired end position (x_{goal}, y_{goal}) may not be reached in one motion, because of that the algorithm was extended with an outer loop and extra logic. The loop and extra logic made the car able to reach the desired end position in more than one motion if that was needed.

An example of the simulations can be seen in figure 33. The thick blue line indicates a parking spot. The red dashed line is the parking perimeter where the car may never cross over for safety reasons. The blue cross is the desired end position w.r.t. the middle of the rear axle. The black shadow is the trace of the car's motion during parking. The cyan line is the trace of the middle of the rear axle. The green dashed line is the end position of the car. The specification of the parking spot is found in the figure caption. $D_{l,offset}$ and $D_{w,offset}$ is the start position offset of the rear middle rear axle w.r.t. the upper right corner of the parking spot. Some parameters were set static according to table 7.

Parameter	Value
u	1 km/h
s_f^{max}	40°
$D_{l,margin}$	0.1 m
$D_{w,margin}$	0.1 m
$D_{w,offset}$	1.0 m
$D_{w,offset}$	$\frac{tw_x}{2} + 0.75$ m.

Table 7: Static parameters.

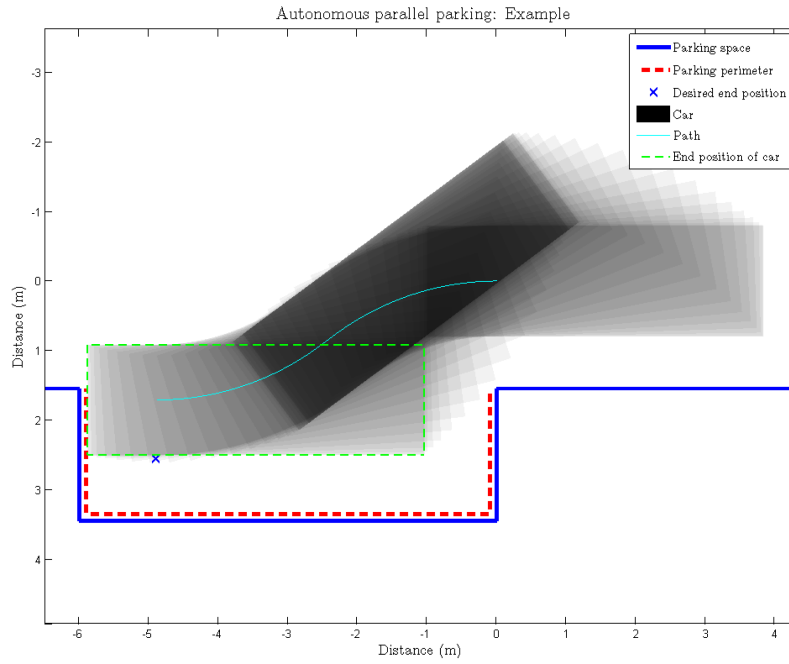


Figure 33: Parallel parking algorithm run once. $s_r^{max} = 0^\circ$, $D_w = 1.9\text{ m}$, $D_l = 6.0\text{ m}$.

The algorithm in figure 33 was iterated just once and did not reach the desired end position in one motion.

In figure 34 and 35 the length of the simulated parking spot was longer, $D_l = 6.3\text{ m}$, and the algorithm iterative. The difference between the simulations is s_r^{max} ; 0° and 10° . To reduce the computational time of the algorithm the constraint of the lateral end position was loosened to $y_{goal} - y_T < 10\text{ cm}$.

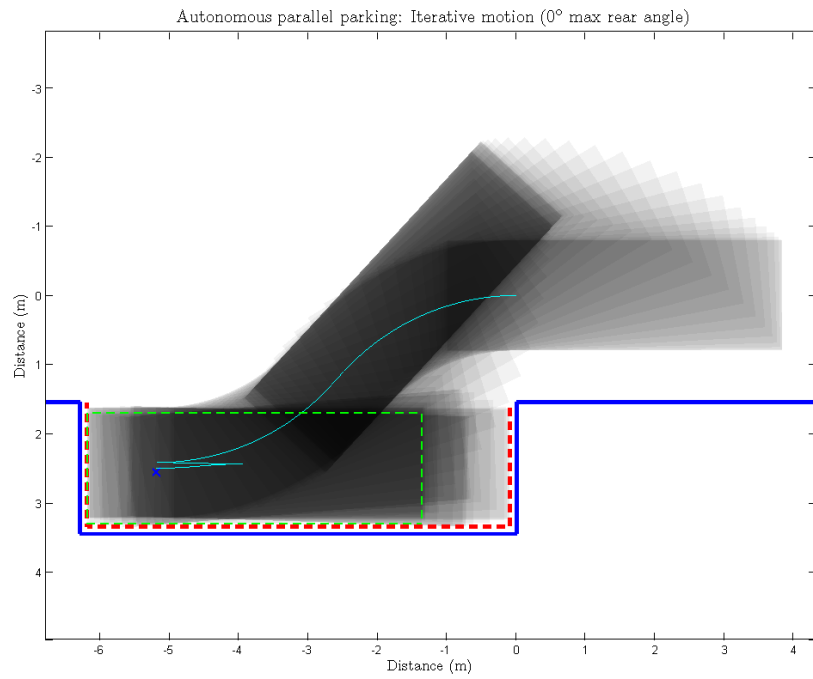


Figure 34: Iterative motion, $s_r^{max} = 0^\circ$, $D_w = 1.9\text{ m}$, $D_l = 6.3\text{ m}$.

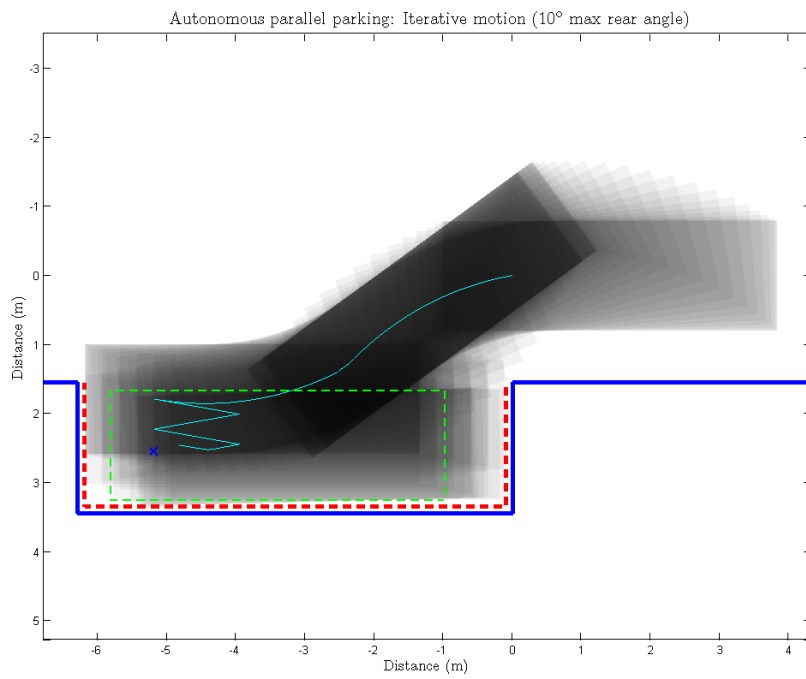


Figure 35: Iterative motion, $s_r^{max} = 10^\circ$, $D_w = 1.9\text{ m}$, $D_l = 6.3\text{ m}$.

With $s_r^{max} = 0^\circ$ the car managed to reach the end position in three iterations, while with $s_r^{max} = 10^\circ$ it took five. In figure 36 a simulation of a parking situation is presented where one iteration of the algorithm was performed with varied max rear steering. The simulation showed that for this parking algorithm the lateral displacement became worse with ARS included.

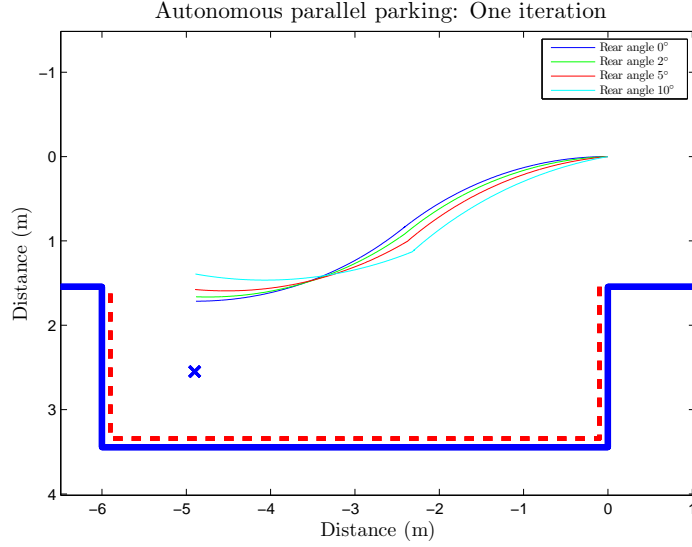


Figure 36: One iteration with varied s_r^{max} , $D_w = 1.9$ m, $D_l = 6.0$ m.

In figure 35 it can be seen that the car was crabbing in iteration 2, 3 and 4, instead of driving in a sinusoidal motion. The lateral travel in these iterations were more than the second iteration in figure 34. Therefore could crabbing be a desired feature to complement the sinusoidal motions.

The lateral displacement per meter driven in longitudinal direction was simulated to investigate the potential of crabbing. The simulation results are presented in table 8.

$s_{f,r}$	Lateral displacement/m
0	0.00
2	0.03
5	0.09
10	0.18

Table 8: Crabbing, lateral displacement/m driven.

Because of the potential of crabbing a combination of activating and deactivating the ARS were developed; when the sinusoidal motion is better than crabbing the ARS will not be activated, but when crabbing is better the ARS will thereby be used and the car will crab.

The simulation results are presented in figure 37. In the simulations D_l were set to 6.0 m . To not clutter the figure the algorithm were just iterated five times and $s_r^{max} = 5^\circ$ was left out. The end position with $s_r^{max} = 5^\circ$ were almost the same as for the position reached in three iterations with $s_r^{max} = 10^\circ$.

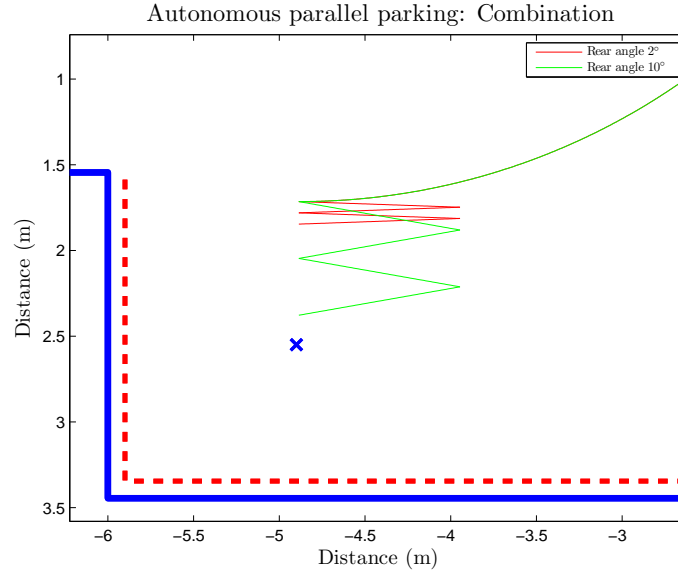


Figure 37: Combination of ARS activation with varied s_r^{max} . $D_w = 1.9\text{ m}$, $D_l = 6.0\text{ m}$.

The simulations run in figure 37 show that for both $s_r^{max} = 2^\circ, 10^\circ$ crabbing is better than the sinusoidal motions in iterations 2 to 5. This shows the potential of crabbing in parallel parking when the rear wheels can be turned at least 5° .

6 Conclusion

In this master thesis the possibilities of implementing ARS in a car was investigated. The results presented in section 5 showed that ARS could have the potential to improve the safety in cars as well as improving the maneuverability and agility. Although ARS had a positive impact in low- and high-speed it did not improve the parallel parking algorithm as expected. When ARS was activated the sinusoidal motions became worse w.r.t. lateral displacement. But if the rear wheels could be turned $\geq 5^\circ$ the crabbing effect is large enough to motivate implementation of ARS in the derived parking algorithm. The ARS could potentially give greater effects if another algorithm is used that does not use two identical, but mirrored, sinusoidal functions.

The derived Two Track model was used as a model of the real car. The validation processes (see section 5.1) showed that the model was accurate enough for its purpose of investigating how ARS impacts the car's behavior. The Two Track model was used to show a proof of concept and present guidelines for an example of a control principle. The Two Track could be used when implementing ARS in reality but it has to be improved with a better modeling of the tires and implement actuator dynamics to begin with. Another approach would be to use the designed control principles (see section 4) with a more sophisticated model such as the VI-CarRealTime model used to validate the Two Track. The better the model becomes the better the control parameters in the real car can be estimated.

From the simulations in lower speeds the maneuverability was increased. For the special case, when driving from a parking spot (see section 5.2.4), the conclusion can be drawn that there was no risk of colliding into the curb or wall when the maximum rear wheel angle was $< 5^\circ$. If the maximum angle would be larger it may cause a problem.

The high-speed simulations, using the LQ-controller, showed that both the reference model and the feedforward gain (K_{ff}) had a large impact on the car's behavior. The reference model "decided" whether the rear wheels would steer in- or off-phase. K_{ff} determined how fast the system would reach steady state; a smaller K_{ff} resulted in a fast system but with overshoots, a larger gain gave a slow system with no overshoots.

Both the reference model and feedforward gain were highly dependent on the velocity and the friction coefficient (μ). With a low μ the reference value from the reference model tended to be too high and the K_{ff} made the system less stable. These are two more things that need to be considered when ARS is implemented in reality.

From the simulation results ARS looks to be a good improvement of today's cars. However, one should consider the difficulty of designing a system virtually; it has to be tested and verified in a physical vehicle in order to reach the desired behavior.

6.1 Future work

Still, there are parts that need to be improved and further work has to be done before implementation of ARS in a real car. In the bullet list below some of the more important work are listed and described.

- The model of the tires could be extended and use the complete model described by Pacejka in [4]. This would more accurately describe the tire forces in the nonlinear regions, skid as an example.
- The dynamics in the actuator, steering the rear wheels, should be implemented to better model the reality. This will probably result in changes in the LQ-controller to get the desired behavior.
- The reference model needs to be modified to better coincide with the reality and make it depend on μ as well. Alternatively derive another model to better estimate the reference signal, for example loop shaping.
- The simulations showed that K_{ff} needed to be depending on both velocity and μ to not get overshoots or a slow system.
- Investigate if more than one LQ-controller (or another controller) must be used. If so, the transitions between these controllers need to be bumpless.
- The yaw rate may not be the ideal state to use as a starting point. Other states may be more suitable to control on and should be studied.

References

- [1] VI-grade, *VI-CarRealTime*, collected 2012-06-04.
http://www.vi-grade.com/index.php?pagid=vehicle_dynamics_carrealtime&SEsviWEB=htun5s0t386h8ii2qfdmki0p7
- [2] I. Paromtchik, C Laugier, *Motion Generation and Control for Parking an Autonomous Vehicle*, (Proc. of the IEEE Int. Conf. on Robotics and Automation), Pages: 3117-3122, 1996.
- [3] H.E. Schouten, *Research the vehicle dynamics of a loaded vehicle*, Technische Universiteit Eindhoven 2005.
- [4] H.B. Pacejka, *Tyre and Vehicle Dynamics*, Butterworth-Heinemann, Amsterdam, 2006.
- [5] T.J. Veldhuizen, *Yaw rate feedback by active rear wheel steering*, Technische Universiteit Eindhoven, 2007.
- [6] S. Widnall, J. Peraire, *Lecture L8 - Relative Motion using Rotating Axes*, Massachusetts Institute of Technology (MIT), Massachusetts, 2009.
- [7] W. Milliken, D. Milliken, *Race Car Vehicle Dynamics*, ISBN-10: 1560915269, 1995.
- [8] N. Bouton, R. Lenain, B. Thuilot, J-C. Fauroux, *A rollover indicator based on the prediction of the load transfer in presence of sliding: application to an All Terrain Vehicle*, Aubie're Cedex, France, 2007.
- [9] G. F. Franklin, J. D. Powell, A. Emami-Naeini, *Feedback Control Of Dynamic Systems, 4:th edition*. Prentice Hall, New Jersey, 2002.
- [10] K. Åström, B. Wittenmark, *Computer Controlled Systems - Theory and Design, 3:rd edition*, ISBN-10: 0486486133, 2002.
- [11] S-J. Chang, S. Tzue-Hseng, *Design and Implementation of Fuzzy Parallel-Parking Control for a Car-Type Mobile Robot* (Journal of Intelligent and Robotic Systems), Pages: 175-194, 2002.
- [12] S-J Huang, G-Y Lin, *Parallel auto- parking of a model vehicle using a self-organizing fuzzy controller* (Journal of Automobile Engineering) Pages: 997-1012, 2006.
- [13] S. Sekhavat, J. Laumond, *Topological property for collision free nonholonomic motion planning: the case of sinusoidal inputs for chained form systems* (IEEE Trans. Autom. Control) Pages: 671-680, 1998.
- [14] K-Z Liu, M.Q Dao, T. Inoue, *An exponentially ϵ -convergent control algorithm for chained systems and its application to automatic parking systems* (IEEE Trans. Control System Technology) Pages: 1113-1126, 2006.
- [15] D. Wang, F. Qi, *Trajectory Planning for a Four-Wheel-Steering Vehicle*, Nanyang Technological University, Singapore, 2001.

A Linear Bicycle model

The linearized state equations of the Bicycle model where F_{yf} and F_{yr} are used as:

$$F_{yf} = C_{stiff_f} \frac{v + a\dot{\psi}}{u} \quad (71)$$

$$F_{yr} = C_{stiff_r} \frac{v - b\dot{\psi}}{u} \quad (72)$$

becomes:

$$\begin{aligned} \dot{v} = & -\frac{1}{u} \left(\frac{C_{stiff_f} + C_{stiff_r}}{m} \right) v \\ & - \frac{1}{u} \left(u^2 + \frac{a * C_{stiff_f} - b * C_{stiff_r}}{m} \right) \dot{\psi} \\ & + \frac{C_{stiff_r}}{m} s_f + \frac{C_{stiff_r}}{m} s_r \end{aligned} \quad (73)$$

$$\begin{aligned} \ddot{\psi} = & -\frac{1}{u} \left(\frac{aC_{stiff_f} - bC_{stiff_r}}{I_z} \right) v \\ & - \frac{1}{u} \left(\frac{a^2 * C_{stiff_f} + b^2 * C_{stiff_r}}{I_z} \right) \dot{\psi} \\ & + \frac{aC_{stiff_r}}{I_z} s_f - \frac{bC_{stiff_r}}{I_z} s_r \end{aligned} \quad (74)$$

B Two Track model: Equations

B.1 Total kinetic energy

Total kinetic energy, T :

$$\begin{aligned} T = & \frac{1}{2} \varphi^2 \dot{\psi}^2 I_y - mu\theta\dot{\varphi}\varphi h' - mu\varphi\dot{\psi}h' - \frac{1}{2}mv\dot{\varphi}\varphi^2 h' \\ & + \frac{1}{2}mu^2 + \frac{1}{2}mv^2 + \frac{1}{2}I_x\dot{\varphi}^2 + \frac{1}{2}I_z\dot{\psi}^2 + \frac{1}{2}m\varphi^2\dot{\psi}^2 h'^2 \\ & + mvh'\dot{\varphi} + \frac{1}{2}I_{xz}\dot{\psi}\theta^2\dot{\varphi} + I_z\theta\dot{\varphi}\dot{\psi} + \frac{1}{2}mh'^2\dot{\varphi}^2 - I_{xz}\dot{\varphi}\dot{\psi} \\ & - \frac{1}{2}I_x\dot{\varphi}^2\theta^2 - I_{xz}\theta\dot{\varphi}^2 + \frac{1}{2}I_z\theta^2\dot{\varphi}^2 + \frac{1}{2}I_{xz}\varphi^2\dot{\psi} - \frac{1}{2}I_z\dot{\psi}^2\varphi^2 \end{aligned} \quad (75)$$

B.2 Derivatives of Lagrange equations of motion

The partial derivatives used in the Lagrange equations (31):

$$\frac{\partial T}{\partial u} = mu - m\theta\dot{\varphi}h' - m\varphi\dot{\psi}h' \quad (76)$$

$$\frac{\partial T}{\partial v} = -\frac{1}{2}m\dot{\varphi}\varphi^2h' + mv + mh'\dot{\varphi} \quad (77)$$

$$\begin{aligned} \frac{\partial T}{\partial \dot{\psi}} &= \varphi^2\dot{\psi}I_y - mu\varphi h' + I_z\dot{\psi} + m\varphi^2\dot{\psi}h'^2 + \frac{1}{2}I_{xz}\theta^2\dot{\varphi} + I_z\theta\dot{\varphi} \\ &\quad - I_{xz}\dot{\varphi} + \frac{1}{2}I_{xz}\varphi^2\dot{\varphi} - I_z\dot{\psi}\varphi^2 \end{aligned} \quad (78)$$

$$\begin{aligned} \frac{\partial T}{\partial \dot{\varphi}} &= mu\theta\varphi h' - \frac{1}{2}mv\varphi^2h' + I_x\dot{\varphi} + mvh' + \frac{1}{2}I_{xz}\dot{\psi}\theta^2 + I_z\theta\dot{\psi} \\ &\quad + mh'^2\dot{\varphi} - I_{xz}\dot{\psi} - I_x\dot{\varphi}\theta^2 - 2I_{xz}\theta\dot{\varphi} + I_z\theta^2\dot{\varphi} + \frac{1}{2}I_{xz}\varphi^2\dot{\psi} \end{aligned} \quad (79)$$

$$\frac{\partial U}{\partial \varphi} = (C_{\varphi f} + C_{\varphi r})\varphi - mgh'\varphi \quad (80)$$

Time derivative of the partial derivatives needed to calculate the Lagrange equations (31):

$$\frac{d}{dt} \frac{\partial T}{\partial u} = -m\theta\ddot{\varphi}h' - m\theta\dot{\varphi}^2h' - m\dot{\varphi}\dot{\psi}h' - m\varphi\ddot{\psi}h' + m\dot{u} \quad (81)$$

$$\frac{d}{dt} \frac{\partial T}{\partial v} = -\frac{1}{2}m\ddot{\varphi}\varphi^2h' - m\dot{\varphi}^2\varphi h' + m\dot{v} + mh'\ddot{\varphi} \quad (82)$$

$$\begin{aligned} \frac{d}{dt} \frac{\partial T}{\partial \dot{\psi}} &= 2\dot{\varphi}\varphi\dot{\psi}I_y + \ddot{\psi}\varphi^2I_y - m\dot{u}\varphi h' - mu\dot{\varphi}h' + I_z\ddot{\psi} + 2m\varphi\dot{\varphi}\dot{\psi}h'^2 \\ &\quad + m\varphi^2\ddot{\psi}h'^2 + \frac{1}{2}I_{xz}\theta^2\ddot{\varphi} + I_z\theta\ddot{\varphi} - I_{xz}\ddot{\varphi} + I_{xz}\varphi\dot{\varphi}^2 \\ &\quad + \frac{1}{2}I_{xz}\varphi^2\ddot{\varphi} - I_z\ddot{\psi}\varphi^2 - 2I_z\dot{\psi}\varphi\dot{\varphi} \end{aligned} \quad (83)$$

$$\begin{aligned} \frac{d}{dt} \frac{\partial T}{\partial \dot{\varphi}} &= m\dot{u}\theta\varphi h' + mu\theta\dot{\varphi}h' - \frac{1}{2}m\dot{v}\varphi^2h' - mv\varphi h\dot{\varphi} + I_x\ddot{\varphi} + m\dot{v}h' \\ &\quad + \frac{1}{2}I_{xz}\ddot{\psi}\theta^2 + I_z\theta\ddot{\psi} + mh'^2\ddot{\varphi} - I_{xz}\ddot{\psi} - I_x\ddot{\varphi}\theta^2 - 2I_{xz}\theta\ddot{\varphi} \\ &\quad + I_z\theta^2\ddot{\varphi} + I_{xz}\dot{\varphi}\varphi\dot{\psi} + \frac{1}{2}I_{xz}\varphi^2\ddot{\psi} \end{aligned} \quad (84)$$

B.3 Final state equations

The final state equations with $\dot{u}, \dot{v}, \ddot{\psi}$ and $\ddot{\varphi}$ as states:

$$\begin{aligned} \dot{u} = & \frac{1}{m} \left(F_{x1} \cos(s_1) + F_{x2} \cos(s_2) + F_{x3} \cos(s_3) + F_{x4} \cos(s_4) \right. \\ & \left. - F_{y1} \sin(s_1) - F_{y2} \sin(s_2) - F_{y3} \sin(s_3) - F_{y4} \sin(s_4) \right) + \theta \ddot{\varphi} \varphi h' \quad (85) \\ & + \theta \dot{\varphi}^2 h' + 2\dot{\varphi} \dot{\psi} h' + \varphi \ddot{\psi} h' + \dot{\psi} \left(-\frac{1}{2} \dot{\varphi} \varphi^2 h' + v \right) \end{aligned}$$

$$\begin{aligned} \dot{v} = & \frac{1}{m} \left(F_{x1} \sin(s_1) + F_{x2} \sin(s_2) + F_{x3} \sin(s_3) + F_{x4} \sin(s_4) \right. \\ & \left. + F_{y1} \cos(s_1) + F_{y2} \cos(s_2) + F_{y3} \cos(s_3) + F_{y4} \cos(s_4) \right) + \frac{1}{2} \ddot{\varphi} \varphi^2 h' \quad (86) \\ & + \dot{\varphi}^2 \varphi h' - h' \ddot{\varphi} - \dot{\psi} \left(-\theta \dot{\varphi} \varphi h' - \varphi \dot{\psi} h' + u \right) \end{aligned}$$

$$\begin{aligned} \ddot{\psi} = & \frac{1}{\varphi^2 I_y - I_z \varphi^2 + I_z + m \varphi^2 h'^2} \left(a(F_{x1} \sin(s_1) + F_{x2} \sin(s_2)) \right. \\ & + a(F_{y1} \cos(s_1) + F_{y2} \cos(s_1)) + M_{z1} + M_{z2} + M_{z3} + M_{z4} \\ & - b(F_{x3} \sin(s_3) + F_{x4} \sin(s_4)) - b(F_{y3} \cos(s_3) + F_{y4} \cos(s_4)) \\ & + \frac{1}{2} t w_r (F_{x3} \cos(s_3) - F_{y3} \sin(s_3)) - \frac{1}{2} t w_r (F_{x4} \cos(s_4) - F_{y4} \sin(s_4)) \\ & + \frac{1}{2} t w_f (F_{x1} \cos(s_1) - F_{y1} \sin(s_1)) - \frac{1}{2} t w_f (F_{x2} \cos(s_2) \\ & - F_{y2} \sin(s_2)) - 2\dot{\varphi} \varphi \dot{\psi} I_y + m \dot{u} \varphi h' - 2m \varphi \dot{\varphi} \dot{\psi} h'^2 - \frac{1}{2} I_{xz} \theta^2 \ddot{\varphi} \\ & - I_z \theta \ddot{\varphi} + I_{xz} \ddot{\varphi} - I_{xz} \varphi \dot{\varphi}^2 - \frac{1}{2} I_{xz} \varphi^2 \ddot{\varphi} + 2I_z \dot{\psi} \varphi \dot{\varphi} \\ & \left. + v \left(-m \theta \dot{\varphi} \varphi h' - m \varphi \dot{\psi} h' \right) - u \left(-\frac{1}{2} m \dot{\varphi} \varphi^2 h' \right) \right) \quad (87) \end{aligned}$$

$$\begin{aligned} \ddot{\varphi} = & \frac{1}{-I_x \theta^2 + m h'^2 + I_z \theta^2 - 2I_{xz} \theta + I_x} \left(-(k_{\varphi f} + k_{\varphi r}) \dot{\varphi} - m \dot{u} \theta \varphi h' \right. \\ & - 2m u \theta \dot{\varphi} h' + \frac{1}{2} m \dot{v} \varphi^2 h' - m \dot{v} h' - \frac{1}{2} I_{xz} \ddot{\psi} \theta^2 - I_z \theta \ddot{\psi} + I_{xz} \ddot{\psi} \\ & - \frac{1}{2} I_{xz} \varphi^2 \ddot{\psi} + \varphi \dot{\psi}^2 I_y - m u \dot{\psi} h' + m \varphi \dot{\psi}^2 h'^2 - I_z \dot{\psi}^2 \varphi \\ & \left. - (c_{\varphi f} + c_{\varphi r}) \varphi + m g h \varphi \right) \quad (88) \end{aligned}$$

C Driving cases

In this section the simulated driving cases are described more in detail. The low speed maneuvers can be found in sections C.1 - C.4, the high speed in C.5 - C.7 and the validation in C.8 - C.9.

C.1 Minimum turn radius

The test shows the minimum turn radius for different maximum rear steer angle. The car has a reference longitudinal speed of 5 km/h and maximum steer angle on both the front and rear wheels off-phase.

C.2 S-curve

In this case the steer angle on front wheels are varied, from maximum steer left to right, and velocity are kept at 5 km/h , which builds up a path that is an S-curve. The ratio between front and rear steer angle are kept at -1, meaning same angle until saturation but in off-phase. The test is repeated with the same input but with varied maximum rear steer angle. The front wheel steer angle over time is illustrated in figure 38.

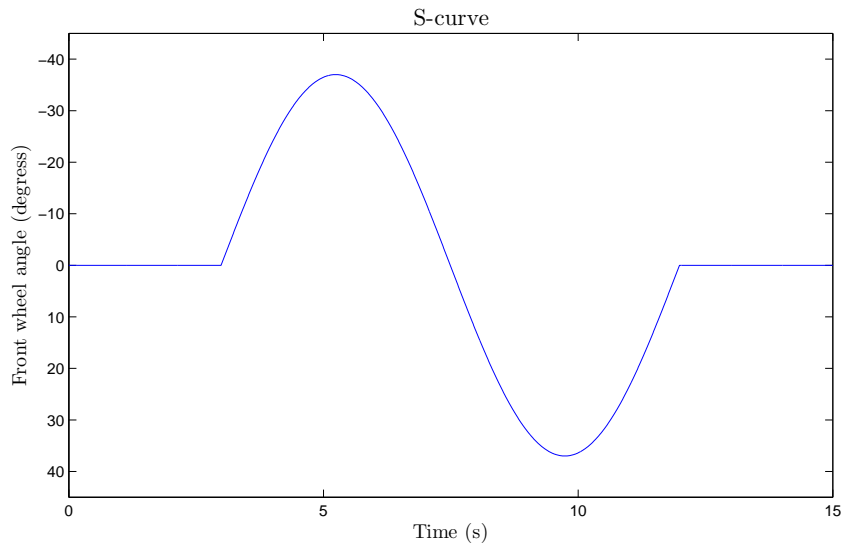


Figure 38: Front wheel steer angle.

C.3 Follow S-curve

This test is similar to the “S-curve”-test (section C.2) but here a predefined path of an S-curve is followed, almost identical to the S-curve produced when ARS was deactivated in the previous section. The velocity is held constant at

5 km/h. The front steer angle is controlled via a PD-controller and the ratio between front and rear wheel angles is kept at -0.5 . The results show the difference in steer angles needed to keep the car on the path.

C.4 Take-off from parallel parking

In this case a simulation of a take-off from a parallel parking spot is performed. The test focuses on the car's lateral displacement of the rear end and wheels. The car accelerates up to 5km/h at the same time the front steer angle is ramped up from 0° to max steer angle in 2 seconds. The maximum rear angle is varied.

C.5 Step steer

The responsiveness of the car is studied in the step steer driving case. The velocity is held constant. The steer angle is ramped up under less than 0.5 seconds to the desired final steer angle and held constant, i.e. the car is driving in a circle.

C.6 Lane change

In this test the stability in a fast lane change on a highway is simulated and studied. The velocity is held constant at 120 km/h and the front wheel angles are illustrated in figure 39, moving the car from the first lane to the one left.

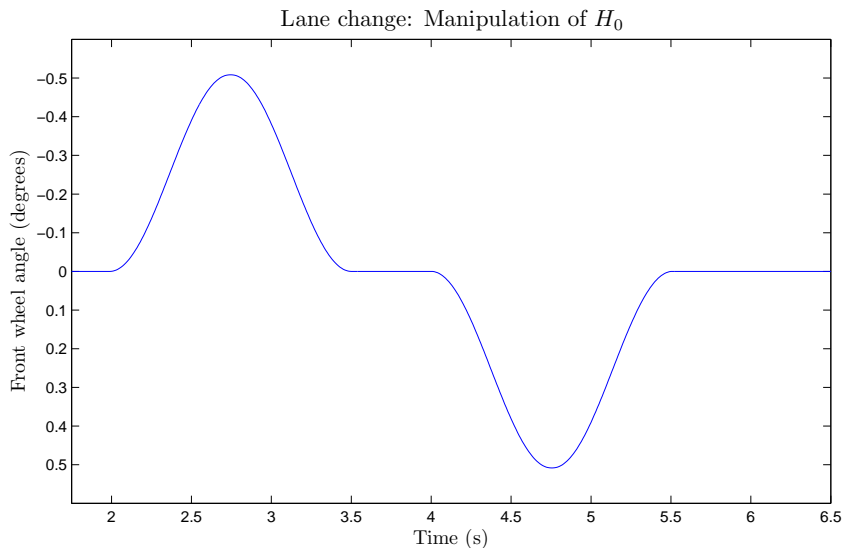


Figure 39: Front wheel angle in a fast lane change.

C.7 External lateral force

An external force in lateral direction is applied to the car meanwhile driving straight forward at constant velocity, 100 km/h . It could be seen as a car on the highway driving on a straight road into a strong wind gust coming from the side.

The lateral force applied to the car is sinus-shaped illustrated in figure 40 and is distributed equally on the four wheels. The force does not described a wind gust correctly, a wind gust is an illustration of the force. The magnitude of the force is chosen as one quarter of the total maximum lateral force (includes all four wheels) from the magic formula.

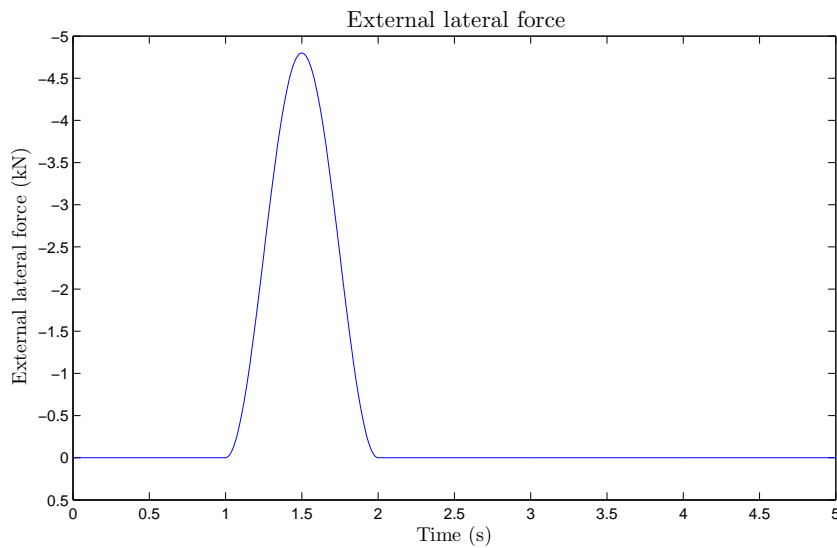


Figure 40: Lateral force that is applied to the car, amplitude may vary.

C.8 Sine 0.5 Hz

In this case the lateral acceleration and yaw rate are examined and the Two Track model's nonlinearities are put to test. The steering wheel input is a sine with 0.5 Hz oscillation with an amplitude of 10° . The velocity is varied from 30 km/h to 180 km/h with steps of 50 km/h .

C.9 Sine with dwell

This driving case is used to objectively determine a vehicle's transient response behavior (yaw rate stability and response) and is similar to an evasive maneuver.

In the beginning of sine with dwell the vehicle holds a constant speed (80 km/h is ISO-standard) and direction. The throttle is released and the steering input shown in figure 41 is executed. The test is repeated with different amplitudes.

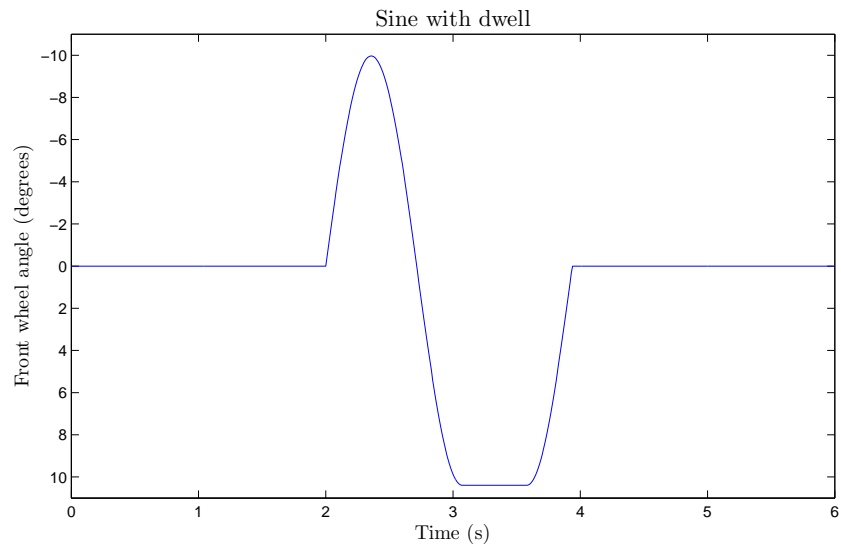


Figure 41: Wheel angle on for sine with dwell driving case (amplitude: 10°).

D Low speed simulations

D.1 Take-off from parallel parking

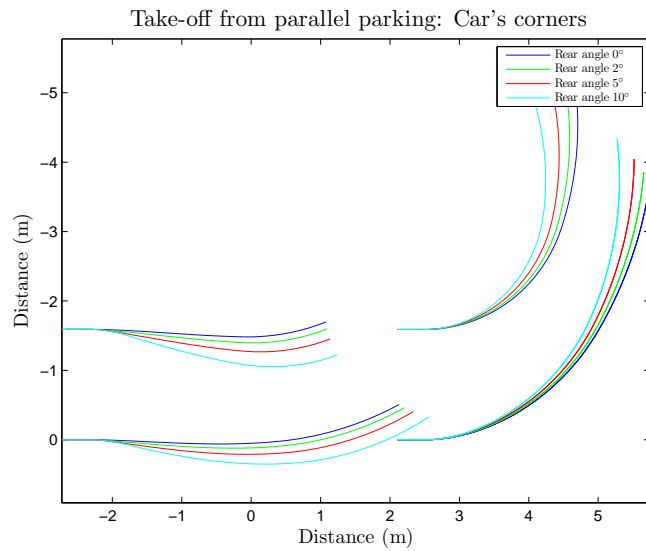


Figure 42: Complete motion of the car's corners while taking off from a parallel parking spot.

E High speed simulations

E.1 Step steer

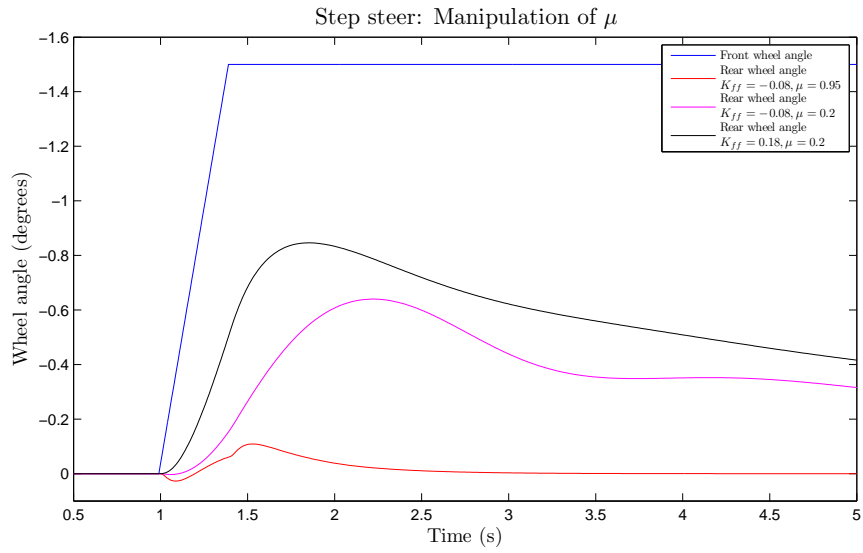


Figure 43: Wheel angles for front and rear wheels, $\mu = 0.20$ and 0.95 .

